Mathematics in Applied Sciences and Engineering
Volume **1**, Number **2**, June **2020**, pp.**126-149**

https://ojs.lib.uwo.ca/mase
https://doi.org/10.5206/mase/8543

A MATHEMATICAL MODEL FOR THE ROLE OF MACROPHAGES IN THE PERSISTENCE AND ELIMINATION OF ONCOLYTIC VIRUSES

NADA ALMUALLEM AND RALUCA EFTIMIE

Abstract. Replicating oncolytic viruses provide promising treatment strategies against cancer. However, the success of these viral therapies depends mainly on the complex interactions between the virus particles and the host immune cells. Among these immune cells, macrophages represent one of the first line of defence against viral infections. In this paper, we consider a mathematical model that describes the interactions between a commonly-used oncolytic virus, the Vesicular Stomatitis Virus (VSV), and two extreme types of macrophages: the pro-inflammatory M1 cells (which seem to resist infection with VSV) and the anti-inflammatory M2 cells (which can be infected with VSV). We first show the existence of bounded solutions for this differential equations model. Then we investigate the long-term behaviour of the model by focusing on steady states and limit cycles, and study changes in this long-term dynamics as we vary different model parameters. Moreover, through local and global sensitivity analysis we show that the parameters that have the highest impact on the level of virus particles in the system are the viral burst size (from infected macrophages), the virus infection rate, and the virus elimination rate.

1. Introduction

Although viral infections are a major health concern to humans and animals, some viruses have been used for therapeutic purposes [36]. An important area where viruses are currently being used to alter the course of the disease is cancer research. In this context, non-replicating viruses have been used as cancer vaccines (by engineering them to express tumour antigens that would trigger an anti-tumour immune response) [33], while replicating viruses have been used either as vaccines that can boost the immune response or as oncolytic agents [51]. Viruses can be naturally oncolytic or can be engineered to display oncolytic activity by genetically modifying them to replicate inside cancer cells and lysing them [49]. However, the efficacy of these viruses is reduced by the presence of anti-viral immune responses. Some of the most important innate immune cells involved in viral clearance are the macrophages.

Macrophages are immune cells that reside in every organ of the body and act as a first line of defence against viral infections [30]. They are also present in large numbers inside various types of solid tumours [29, 56], and thus they are likely interfering with viral therapies for cancers [10]. In the context of viral infections, macrophages can eliminate viruses and virus-infected cells through phagocytosis [32]. They can also enhance the spread of different infections, as some viruses infect and replicate inside these cells [31, 43, 44]. Macrophages are a very heterogeneous cell population, with the two extreme phenotypes being represented by the pro-inflammatory classically-activated M1 cells, and the anti-inflammatory alternatively-activated M2 cells [30, 52]. Different macrophages phenotypes respond differently to viral infections. For example, the influenza virus seems to replicate better inside the M2 cells compared to the M1 cells [12]. Moreover, some viral infections seem to affect the macrophages polarisation. For example, the human immunodeficiency virus (HIV) infection can switch the phenotype of infected macrophages towards an M2-like phenotype during the later stages of the disease [27, 52], while the human cytomegalovirus (HCMV) skews the phenotype of infected macrophages towards an

Received by the editors 10 January 2020; 4 April 2020; accepted 5 April 2020; published online 8 April 2020.
2000 *Mathematics Subject Classification.* Primary 34A12, 92-08; Secondary 34C23, 34C60 .
Key words and phrases. mathematical modelling; oncolytic VSV; M1 macrophages; uninfected M2 macrophages; infected M2 macrophages.

M1-dominated phenotype which might support their replication and spread [6]. Some oncolytic viruses can also induce the switch of macrophages towards an M1-like phenotype, by increasing the expression of pro-inflammatory cytokine interferon-γ (IFN-γ) [45].

In this study we focus on replication-competent Vesicular Stomatitis Virus (VSV) vectors, which have been shown to offer great promise as oncolytic agents mainly because (i) they are not pathogenic to humans and (ii) humans do not have pre-existing immunity against these viruses [26, 3]. In regard to the interactions between these virus particles and the macrophages, various experimental studies have shown that immune protection against VSV infection is controlled by the induction of a type-I interferon response [53], and therefore, the M1 macrophages are likely to be involved in the elimination of VSV particles. Moreover, it is known that macrophages can be infected by the VSV [50, 54]. An experimental study in [38] suggested that the M2 macrophages can support viral replication, while the M1 macrophages are resistant to infection with VSV. Other experimental studies (which do not differentiate between M1 and M2 cells) have suggested that macrophages can act as a reservoir for VSV, not encouraging viral replication [54]. In [22] it was shown that in the context of breast cancer, a VSV strain can modulate macrophages phenotype from a M2-like phenotype towards an M1-like phenotype. This is probably due to the induction of a type-I interferon response after VSV infection, which stimulates innate immune cells [55]. Therefore, it seems that there is a fine balance between the roles of VSV in inducing an innate immune response and escaping this anti-viral immune response (which is particularly important in the context of various diseases, such as cancers that can be infiltrated by large numbers of macrophages). Because experimental studies do not offer a full understanding of this delicate balance, in this paper we consider a mathematical modelling approach to further investigate this aspect.

Mathematical and computational approaches have been used over the past years to investigate the interactions between viruses and macrophages in the context of cancer [9, 13, 14, 35, 37], or in the context of different viral infections [5, 17, 18, 21, 25, 28, 34, 41, 61]. While the latest models that focus on oncolytic viruses differentiate between the anti-tumour and anti-viral roles of M1 and M2 macrophages, the models that focus on viral infections do not usually differentiate between the roles of M1 and M2 cells in eliminating/spreading the infection. Among the few models that focus on the different roles of M1 and M2 cells during viral infections we mention [34, 21]. Regarding macrophages response to oncolytic viruses, including VSV, to our knowledge there are no mathematical models that focus on the infection of macrophages with these viruses, and on the delicate balance between the anti-viral immunity and macrophages support for a viral reservoir or viral replication.

The main goal of this study is to derive a mathematical model that can shed light on the complex interactions between the M1 and M2 macrophages and the VSV particles. In particular, we aim to answer the following question: What mathematical and biological mechanisms can lead to a decrease/increase in viral titres? (An increase in viral titres is important in the context of oncolytic therapies for cancer, while a decrease in these titres is important for avoiding chronic infections.)

The structure of this work is as follows. In Section 2, we introduce a mathematical model for the interactions between M1/M2 macrophages and VSV particles. In Section 3, we discuss the non-negativity and boundedness of solutions, as well as the long-term behaviour of the model through the investigation of the number and stability of steady states. We also perform a local sensitivity analysis to investigate the role of different model parameters on the overall viral load. We conclude in Section 4 with a summary and discussion of the results.

2. Model Description

The graphical description of the proposed mathematical model is shown in Figure 1. We define four variables: the density of M1 macrophages (M_1) (which are resistant to VSV infection [48]), the densities of uninfected M2 macrophages (M_{2u}) and VSV-infected M2 macrophages (M_{2i}) [48], and the density of oncolytic virus particles (V). We emphasise that in this study, even if we focus on oncolytic viruses, we ignore their interactions with the tumour cells and focus exclusively on the interactions of these viruses with the macrophages. The time-evolution of these variables is given by the following

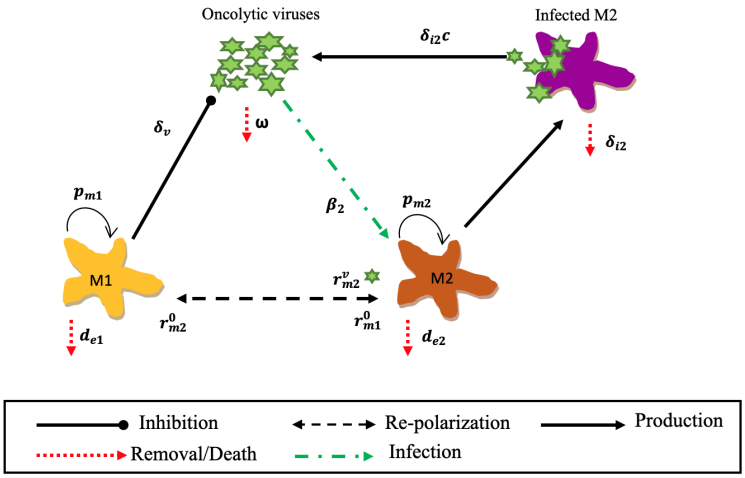

FIGURE 1. Description of the interactions between the M1/M2 macrophages and an oncolytic VSV, as given by equations (2.1a)-(2.1d). The model was inspired by the experimental studies in [50, 38, 48] (where the VSV infects only the M2 cells but not the M2 cells), and the mathematical modelling studies in [13, 14] (which focused only on the anti-viral effect of M1 cells, and did not consider the infection of macrophages). Even if we focus on an ocolytic virus, here we do not investigate the effect of the tumour on these VSV-macrophages interactions; this aspect will be investigated in a further study [2].

differential equations:

$$\frac{dM_1(t)}{dt} = \underbrace{p_{m1}M_1(t)\left(1-\frac{M_1(t)+M_{2u}(t)}{k_2}\right)}_{logistic\ growth} - \underbrace{r^0_{m1}M_1(t)}_{M1\to M2\ polarisation} + \underbrace{M_{2u}(t)\left(r^0_{m2}+r^v_{m2}\frac{V(t)}{h_v+V(t)}\right)}_{M2\to M1\ re-polarisation} - \underbrace{d_{e1}M_1(t)}_{natural\ death}, \tag{2.1a}$$

$$\frac{dM_{2u}(t)}{dt} = \underbrace{p_{m2}M_{2u}(t)\left(1-\frac{M_1(t)+M_{2u}(t)}{k_2}\right)}_{logistic\ growth} + \underbrace{r^0_{m1}M_1(t)}_{M1\to M2\ polarisation} - \underbrace{M_{2u}(t)\left(r^0_{m2}+r^v_{m2}\frac{V(t)}{h_v+V(t)}\right)}_{M2\to M1\ re-polarisation} - \underbrace{\beta_2V(t)M_{2u}(t)}_{M2\ infection\ with\ VSV} - \underbrace{d_{e2}M_{2u}(t)}_{natural\ death}, \tag{2.1b}$$

$$\frac{dM_{2i}}{dt} = \underbrace{\beta_2V(t)M_{2u}(t)}_{M2\ infection\ with\ VSV} - \underbrace{\delta_{i2}M_{2i}(t)}_{lysis\ by\ viruses}, \tag{2.1c}$$

$$\frac{dV}{dt} = \underbrace{c\delta_{i2}M_{2i}(t)}_{production\ of\ viruses} - \underbrace{\delta_vV(t)\frac{M_1(t)}{h_m+M_{2u}(t)}}_{virus\ elimination\ by\ M1} - \underbrace{\omega V(t)}_{natural\ death}, \tag{2.1d}$$

with the initial conditions

$$M_1(0) \geq 0, \quad M_{2u}(0) \geq 0, \quad M_{2i}(0) \geq 0, \quad V(0) \geq 0. \tag{2.2}$$

This model incorporates the following biological assumptions:

- In Eqns. (2.1a)-(2.1b), the M1 and uninfected-M2 macrophages grow logistically at rates p_{m1} and p_{m2} through a self renewal process [30] up to a maximum carrying capacity k_2. This type of growth depicts experimentally observed cell kinetics [7]. To describe macrophages plasticity, we assume that the environment can induce a M1→M2 polarisation at a constant rate r^0_{m1} (e.g., in the presence of cytokines such as IL-4, IL-10 [1]), or a M2→M1 re-polarisation at a constant rate r^0_{m2} (e.g., in the presence of cytokines such as IFN-γ, IL-2 [1]). Moreover, it has been experimentally shown in [22] that matrix (M) protein mutant (rM51R-M) VSV could modulate the switch M2→M1 (probably through the induction of IFN-γ response). Furthermore, engineering oncolytic viruses which carry specific cytokines can trigger a macrophages re-polarisation to a M1-like phenotype [24]. Thus, we assume that this enhanced M2→M1 re-polarisation occurs at a rate r^v_{m2} in the presence of the virus. The re-polarisation of M2 cells upon contact with VSV particles is described by a Michaelis-Menten term with constant h_v to account for the saturated re-polarising response induced by viruses. The M1 and M2 macrophages have natural mortality rates d_{e1} and d_{e2}, respectively. Finally, the M2 macrophages are predisposed to infections with VSV particles at a rate β_2 [48], while the M1 cells are resistant to VSV infections [48].
- In Eq. (2.1c), the infected M2 macrophages are eliminated by the viruses at a rate δ_{i2}. All other terms have been described above.
- In Eq. (2.1d), we assume that each infected M2 macrophage releases c new VSV particles [22]. Moreover, the reduction in the number of virus particles is the result of their elimination, at a rate δ_v, by the M1 macrophages. Note that, as discussed in [10], viral clearance may be prevented by the M2 macrophages. Finally, we assume that the virus particles have a natural death rate ω [11]. This last term includes also the virus elimination rate by other innate immune cells (e.g., NK cells [58]) or adaptive immune cells (e.g., T cells [8]) not considered in this study.

All parameters that appear in model (2.1) are non-negative and described in further detail in Table 2.

Remark 2.1. Since many experimental studies on the proliferation rates of macrophages do not distinguish between the M1 and M2 cells [7], throughout most of this study we will assume that $p_{m1} = p_{m2} =: p_m$. For simplicity we also assume that $d_{e1} = d_{e2} =: d_e$. The cases where $d_{e1} \neq d_{e2}$ and $p_{m1} \neq p_{m2}$ will be investigated in Section 3.3.

Remark 2.2. For the macrophages logistic proliferation terms, one could include also the infected macrophages that produce virus particles: $p_{m1,m2}M_{1,2u}\left(1 - \frac{M_1+M_{2u}+M_{2i}}{k_2}\right)$. However, some experimental studies have shown that the proportion of productively infected cells is very small: only 0.9-7.5% of the total cells were able to produce viruses [50]. Therefore, in this study we ignore the variable M_{2i} from the proliferation terms, since it does not impact them significantly.

TABLE 1. Summary of initial conditions used for numerical simulations of system (2.1). By choosing these conditions, we tried to replicate the experimental conditions from [50].

Variable	Description	Initial condition
M_1	Density of M1 macrophages (cell numbers per volume)	$M_1(0) = 4 \times 10^5$
M_{2u}	Density of uninfected M2 macrophages (cell numbers per volume)	$M_{2u}(0) = 1 \times 10^5$
M_{2i}	Density of infected M2 macrophages (cell numbers per volume)	$M_{2i}(0) = 0$
V	Density of virus particles (particles forming units (PFU) per volume)	$V(0) = 5 \times 10^1$

2.1. **Parameter values.** In Table 2, we summarise the parameter values used throughout this theoretical study. Some of these values were taken directly from the existent mathematical literature, while other values (marked by "*" in Table 2) were approximated based on experimental studies – see the discussion below. However, there were a few parameters for which we could not find any values, so we provided some estimated ranges (see Table 2). In the following we discuss the parameter values we approximated using experimental studies, and the values taken from the literature (especially if different mathematical studies used different parameter values).

- In [19] the authors suggested that the doubling time of macrophages is around 27hrs. In [66] the authors estimated the doubling time of untreated murine macrophage-like RAW264.7 cells to be between $18-22$hrs, while cells stimulated with bacterial lipopolysaccharide (LPS) had an estimated doubling time of 35hrs. In [57], the authors estimated that M1 macrophages have a doubling time between 23.86hrs and 28.97hrs. In [7] it has been indicated that the average doubling time of macrophages is between $20-30$hrs. From all these experimental studies we can conclude that the doubling time of macrophages is likely between $18-35$hrs, which corresponds to proliferation rates between $0.4-0.9$/day. For simplicity, through this study we choose $p_{m1}=p_{m2}=0.57$/day.
- In regard to the M1/M2 macrophages death rates, various modelling studies used different values. For example, in [15] it was assumed that $d_{e1}=d_{e2}=0.02$/day, the same as in [40]. On the other hand, in [13] the authors considered $d_{e1}=d_{e2}=0.2$/day, as approximated from the experimental study in [63]. Here, we use the same values as in [13], i.e. $d_{e1}=d_{e2}=0.2$/day. However, in Section 3.3 we will assume different macrophages death rates (i.e., $d_{e1}=0.1$ and $d_{e2}=0.8$) and investigate their impact on the dynamics of the system.
- Various experimental studies investigated macrophages yield per mouse. For example, in [64] the authors isolated macrophages from bone marrow, spleen and peritoneal cavity, and the numbers varied between 10^6-10^7 cells per site. Throughout this study we use the same carrying capacity for macrophages as in [13, 15]: $k_2=10^8$ cells.
- In regard to the apoptosis rate of infected macrophages, Rager *et. al* [50] showed that two macrophages cell lines (clones J774.16 and C3C, derived from the murine reticulum cell sarcoma J774) were completely lysed by the virus within 1-2 days after infection. Thus, we assume a death rate of $\delta_{i2}\in\left(\frac{\ln(2.0)}{2},\frac{\ln(2.0)}{1}\right)=(0.35,0.69)$/day. For the simulations we use an average value of $\delta_{i2}=0.52$.
- In regard to the virus burst size, [50] showed that each productively infected macrophage was able to produce viral progeny of at least 1000PFU. Moreover, Zhu *et. al* [65] showed that each virus-infected cell produced between 50 to 8000 progeny virus particles. For our simulations we use an average of $c=2500$, which is the same value as in [13].
- The VSV death rate varies between different mathematical studies: e.g., $\omega=2$/day in [13, 39]), or $\omega\in(1-2.56)$/day in [16]. This is because experimental studies have shown that the intracellular half-lives of non-replicating wild type and mutant strains of VSV can vary between 5.3hrs and 18hrs, which translates into a death rate between $\ln(2)/5.3$hr$=3.13$/day and $\ln(2)/18$hr$=0.92$/day [11]. In [23] the authors have calculated the half-life of a replicating VSV strain between $2-15.9$hrs, which translates into a death rate between $1.04-8.31$/day. In this study, we choose an average death rate of $\omega=2$/day.
- In regard to the M1→M2 and M2→M1 polarisation rates, the theoretical studies in [59, 15] used $r^0_{m1}\in(0.05,0.09)$ and $r^0_{m2}\in(0.05,0.08)$. In [13] the authors used the baseline values of $r^0_{m1}=0.001$ and $r^0_{m2}=0.01$, which could vary between $(0.0001,0.1)$. Here, we use the same parameter ranges as in [13].
- The rest of the parameter values (i.e., r^v_{m2}, h_m, h_v, β_2, δ_v) used in this study for the numerical simulations are listed in Table 2.

TABLE 2. Summary of the parameters that appear in model (2.1), together with the values used for the numerical simulations. References marked by "*" correspond to parameter values that were approximated based on experimental studies. Some of the items in column "Value" show the ranges over which those parameters were varied, while the parentheses show the baseline values used for the numerical simulations.

Param.	Description	Value	Units	Reference
p_{m1}	proliferation rate of M1 cells	0.4 – 0.9 (0.57)	days^{-1}	*[19],[66], [57]
p_{m2}	proliferation rate of M2 cells	0.4 – 0.9 (0.57)	days^{-1}	*[19],[66], [57]
β_2	infection rate of M2 macrophages with the oncolytic virus	$2\times10^{-5}-2$ (0.000002)	days^{-1} (PFU/vol)$^{-1}$	estimated
δ_{i2}	rate at which an infected M2 are killed by viruses	0.35 – 0.69 (0.52)	days^{-1}	*[50]
c	number of virus particles released from an infected M2 cell	50 – 8000 (2500)	PFU/cells	[65]
ω	death rate of oncolytic virus particles	0.1-10 (2.0)	days^{-1}	[13, 39],[11, 23]
δ_v	elimination rate of viruses by the M1 cells	5×10^{-5}–0.5 (5×10^{-5})	days^{-1}	estimated
k_2	carrying capacity of macrophages	10^6 – 10^9 (10^8)	cells/vol	[13]
r^0_{m1}	M1→M2 re-polarisation rate in response to cytokines in the microenvironment	$0.00001-0.1$ (0.001)	days^{-1}	[13],[59]
r^0_{m2}	M2→M1 re-polarisation rate in response to cytokines in the microenvironment	$0.00001-1.0$ (0.01)	days^{-1}	[13],[59]
r^v_{m2}	M2→M1 re-polarisation rate in response to engineered viruses	$0-10$ (0.0)	days^{-1}	estimated
d_{e1}	natural death rate of M1 macrophages	0.02 – 0.8 (0.2)	days^{-1}	[13],[63]
d_{e2}	natural death rate of M2 macrophages	0.02 – 0.8 (0.2)	days^{-1}	[13],[63]
h_v	half-saturation constant for the viruses to trigger a M2 → M1 re-polarisation	0.2 – 1.7 (1.0)	PFU/vol	estimated
h_m	half-saturation constant for macrophages that support half the maximum immune response	0.2 – 1.7 (1.0)	cells/vol	estimated

3. RESULTS

To understand the dynamics of system (2.1), we first show that the model is well-posed and biologically realistic. Then we focus on the steady states and their stability to investigate the long-term behaviour of the system. We also perform numerical simulations to confirm these analytical results, and to test the impact of different parameters on the transient and long-term behaviour of the mathematical model.

3.1. Non-negativity and boundedness of solutions.

We start the investigation of model (2.1a)-(2.1d) by showing that it is biologically realistic, in the sense that all cell and virus populations are non-negative and bounded.

Proposition 3.1. The following results hold true:

(i) There exists a unique solution $(M_1, M_{2u}, M_{2i}, V) \in \mathbb{R}^4_{\geq 0}$ for system (2.1a)-(2.1d).

(ii) For any $(M_1, M_{2u}, M_{2i}, V) \in \mathbb{R}^4_{\geq 0}$ there exists a nonnegative solution to system (2.1a)-(2.1d) for all $t \geq 0$. Moreover, there exist positive constants L_1, L_2 and L_3 independent of initial data, such that $M_1 + M_{2u} \leq L_1$, $M_{2i} \leq L_2$ and $V \leq L_3$ for sufficiently large t.

Proof. See Appendix A. □

3.2. **Long-term dynamics: steady states and stability.** We begin investigating the long-term behaviour of the model (2.1a)-(2.1d) by discussing all possible steady states. The equilibria of (2.1a)-(2.1d) satisfy the following equations:

$$p_{m1}M_1^*\left(1-\frac{M_1^*+M_{2u}^*}{k_2}\right)-d_{e1}M_1^*-r_{m1}^0M_1^*+M_{2u}^*\left(r_{m2}^0+r_{m2}^v\frac{V^*}{h_v+V^*}\right)=0, \tag{3.1a}$$

$$p_{m2}M_{2u}^*\left(1-\frac{M_1^*+M_{2u}^*}{k_2}\right)-\beta_2V^*M_{2u}^*-d_{e2}M_{2u}^*+r_{m1}^0M_1^*-M_{2u}^*\left(r_{m2}^0+r_{m2}^v\frac{V^*}{h_v+V^*}\right)=0, \tag{3.1b}$$

$$\beta_2V^*M_{2u}^*-\delta_{i2}M_{2i}^*=0, \tag{3.1c}$$

$$c\delta_{i2}M_{2i}^*-\omega V^*-\delta_vV^*\frac{M_1^*}{h_m+M_{2u}^*}=0. \tag{3.1d}$$

As mentioned in the previous section, since we do not have data which differentiates between the proliferation rates for M1 and M2 cells, we assume that $p_{m1}=p_{m2}:=p_m$. For simplicity we also assume for now that $d_{e1}=d_{e2}:=d_e$. Under these assumption, model (2.1) exhibits three types of equilibria:

(i) *Immune-Free Virus-Free Steady State (IVF)*: $(M_1^*,M_{2u}^*,M_{2i}^*,V^*)=(0,0,0,0)$.
(ii) *Immune-Present Virus-Free Steady State (VF)*: $(M_1^*,M_{2u}^*,M_{2i}^*,V^*)=(M_1^*,M_{2u}^*,0,0)$.
(iii) *Immune-Present Virus-Present Steady State (IV)*: $(M_1^*,M_{2u}^*,M_{2i}^*,V^*)=(M_1^{*,v},\ M_{2u}^{*,v},\ M_{2i}^{*,v},\ V^{*,v})$.

In the following, we obtain explicit expressions for the equilibria (ii) and (iii). To this end, note that solving Eq. (3.1c) for M_{2i}, and further substituting this solution into Eq. (3.1d) leads to

$$V^*\left(c\beta_2M_{2u}^*-\delta_v\frac{M_1^*}{h_m+M_{2u}^*}-\omega\right)=0, \tag{3.2}$$

which means that

$$\text{either}\ \ V^*=0\quad\text{or}\quad M_1^*=\frac{(c\beta_2M_{2u}^*-\omega)(h_m+M_{2u}^*)}{\delta_v}. \tag{3.3}$$

- If $V^*=0$: then $M_{2i}^*=0$ (from Eq. (3.1c)), and thus we can obtain an explicit expression for the steady state (ii) by solving Eqns. (3.1a) and (3.1b) for non-zero M_1^* and M_{2u}^* values:

$$M_1^*=\frac{(p_m-d_e)k_2r_{m2}^0}{(r_{m1}^0+r_{m2}^0)p_m},\quad M_{2u}^*=\frac{(p_m-d_e)k_2r_{m1}^0}{(r_{m1}^0+r_{m2}^0)p_m}. \tag{3.4}$$

  Both M_1^* and M_{2u}^* exist when the proliferation rate of macrophages is greater than their death rate (i.e., $p_m>d_e$).
- If $V^*\neq0$: we can obtain an expression for the steady state (iii), by adding Eqns. (3.1a) and (3.1b), to obtain an implicit equation in M_{2u}^*, M_1^* and V^*,

$$p_m(M_1^*+M_{2u}^*)\left(1-\frac{M_1^*+M_{2u}^*}{k_2}\right)-d_e(M_1^*+M_{2u}^*)-\beta_2V^*M_{2u}^*=0, \tag{3.5}$$

  and then substituting M_1^* from Eq. (3.3) into Eq. (3.5). This yields a polynomial of the fourth degree in M_{2u}^* (with M_{2u}^* seen as a function of V^*):

$$P(M_{2u}^*):=A(M_{2u}^*)^4+B(M_{2u}^*)^3+C(M_{2u}^*)^2+(D+EV^*)(M_{2u}^*)+F=0, \tag{3.6}$$

where

$$A = p_m c^2 \beta_2^2, \quad B = 2cp_m\beta_2(ch_m\beta_2 - \omega + \delta_v),$$
$$C = \left[\delta_v^2 + \left(2c(h_m - \frac{k_2}{2})\beta_2 - 2\omega\right)\delta_v + c^2h_m^2\beta_2^2 - 4ch_m\beta_2\omega + \omega^2\right]p_m + cd_ek_2\beta_2\delta_v,$$
$$D = (c\beta_2 h_m - \omega + \delta_v)\left[k_2\delta_v(d_e - p_m) - 2h_m\omega p_m\right],$$
$$E = \beta_2 k_2 \delta_v^2, \qquad F = h_m^2\omega^2 p_m + \omega h_m k_2 \delta_v(p_m - d_e).$$

Only real positive solutions $M_{2u}^{*,v}$ of Eq. (3.6) provide biologically relevant steady states. For the parameter values used here (i.e., $p_m > d_e$, so that this state exists; see Proposition 3.2) there are either zero or two positive solutions $M_{2u}^{*,v}$ for each $V^{*,v}$ (see Figure 2(a)), and correspondingly two positive solutions $M_{2i}^{*,v}$ for each $V^{*,v}$, with $M_{2i}^{*,v} = (\beta_2 V^{*,v} M_{2u}^{*,v})/\delta_{i2}$ (see Figure 2(b)). To obtain a better understanding of the effect of different virus-related and immune-related parameters on these coexistence steady states, in Figure 2 we graph $M_{2u}^{*,v}$ vs. $V^{*,v}$ (and $M_{2i}^{*,v}$ vs. $V^{*,v}$) as we vary: (i) β_2, (ii) c, (iii) ω, (iv) p_m, (v) d_e, (vi) δ_v. We observe that variations in some parameters (e.g., p_m, d_e, δ_v) do not impact in a similar manner the two (IV) states, with a more significant impact being observed on the state characterised by a larger M_{2u}^* (i.e., the upper branch of these plots).

In Figure 2 we also observe that these non-zero (IV) states exit only for smaller V^* values: when $V^* > 10^{10}$ there are no such immune-present virus-present states. This observation is detailed in the last part of Proposition 3.2, and proved in Appendix B.

The following result summarises the conditions for the existence and stability of the steady states exhibited by model (2.1) (under the assumption that $p_{m1} = p_{m2} = p_m$ and $d_{e1} = d_{e2} = d_e$):

Proposition 3.2. Model (2.1) can have three different types of steady states, with the following stabilities:

(i) The Immune-Free Virus-Free Steady State (IVF), which exists for all non-zero parameter values and is locally asymptotically stable when $p_m \le d_e$ and unstable otherwise.

(ii) The Immune-Present Virus-Free Steady State (VF), which exists for $p_m > d_e$ and is locally asymptotically stable when

$$R_e^0 := \frac{c\beta_2 M_{2u}^*}{\delta_v \frac{M_1^*}{h_m + M_{2u}^*} + \omega} < 1, \tag{3.7}$$

and unstable otherwise.

(iii) The Immune-Present Virus-Present Steady States (IV) (with $p_{m1} = p_{m2} = p_m$ and $d_{e1} = d_{e2} = d_e$) exist provided that $p_m > d_e$, $M_{2u}^* > \omega/(\beta_2 c)$ and $V^* < -D/E$ (with $D < 0$ and E given by Eq. (3.6)). These states can be stable or unstable, depending on model parameters.

Proof. See Appendix B. □

All these existence and stability results for the steady states displayed by model (2.1) are summarised in Figure 3. Here we vary the cells proliferation rates p_m above/below the death rates $d_e = 0.2$, since these two parameters control the stability of the (IVF) state and the existence of the (VF) and (IV) states. In sub-panel (i) we graph M_{2u}^* vs. p_m, while in sub-panel (ii) we graph V^* vs. p_m. Figure 3 shows that the (IVF) steady state is stable when $p_m \in (0, 0.2)$ and unstable when $p_m \in (0.2, 0.9)$. The steady states (VF) and (IV) do not exist for $p_m < d_e = 0.2$; they exist only for $p_m \ge d_e = 0.2$. Moreover, for the baseline parameter values in Table **??**, the (VF) steady state is unstable when it exists, while for the two co-existence (IV) states one is stable and the other one is unstable (see also Figure 10 in Appendix B).

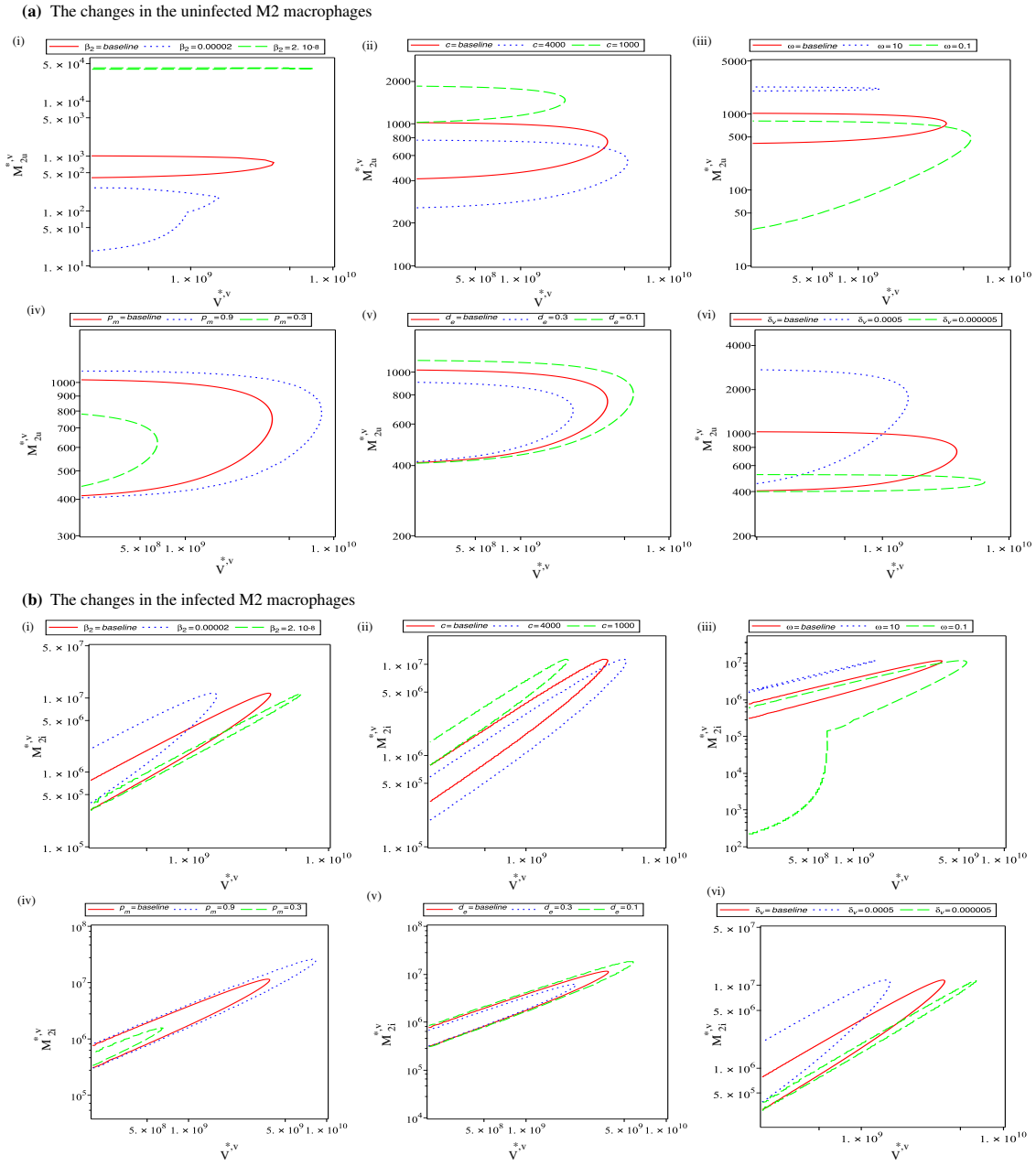

FIGURE 2. Immune-Present Virus-Present Steady State (IV) $(M_1^{*,v}, M_{2u}^{*,v}, M_{2i}^{*,v}, V^{*,v})$: the curves in (a) show the uninfected M2 cells (given by Eq. (3.6)) as a function of virus particles V^*, while the curves in (b) show the infected M2 cells as a function of V^* (where $M_{2i}^* = \beta_2 V^* M_{2u}^*/\delta_{i2}$). In sub-panels (i)-(vi) we investigate the changes in these steady states (IV) as we vary (i) the infection rate β_2, (ii) the burst size c, (iii) the decay rate ω, (iv) the proliferation rate p_m, (v) the death rate d_e and (vi) the elimination rate of viruses by M1 cells δ_v. The rest of parameters are fixed at their baseline values shown in Table 2.

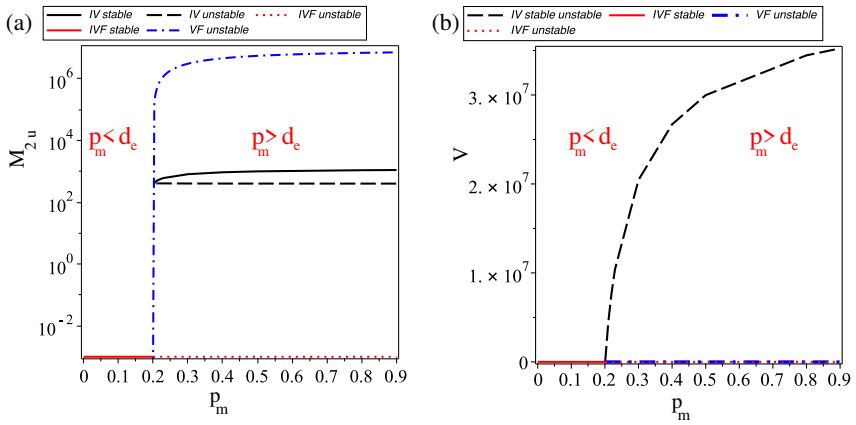

FIGURE 3. Summary of all possible steady states and their stability, as determined by the relation between p_m and d_e; (a) M_{2u}^* vs. p_m; (b) V^* vs. p_m. Note that the (IVF) state is stable when $p_m < d_e$. The (VF) state exists when $p_m > d_e = 0.2$; moreover, when it exists is unstable ($R_e^0 > 1$). The co-existence (IV) state exists when $p_m > d_e = 0.2$. The rest of parameter values are as described in Table 2.

In Figure 4 we show numerically the dynamics of system (2.1) as the solutions approach the three steady states discussed above, for some specific parameters values which ensure that these states are stable (and thus the solution trajectories will approach them).

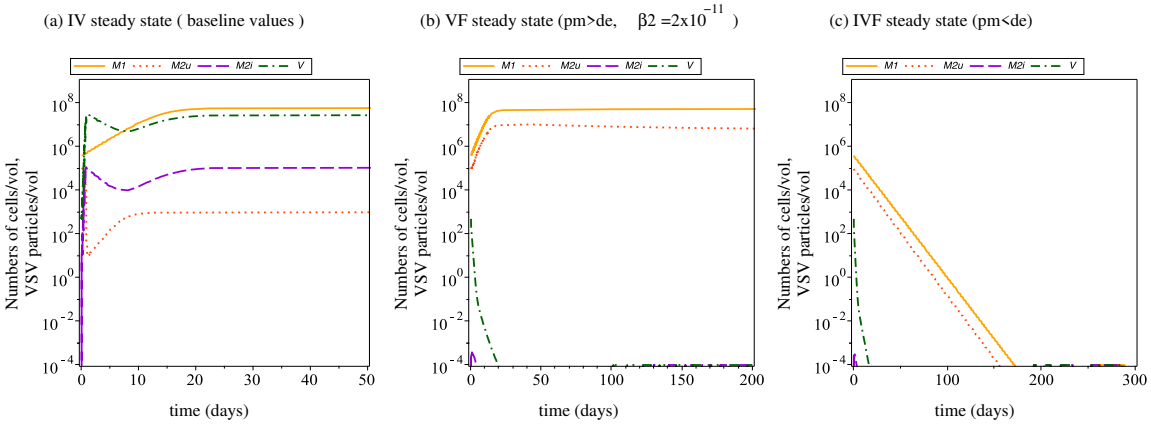

FIGURE 4. Dynamics of model (2.1) as the solutions approach asymptotically the three steady states: (a) For the baseline parameter values (see Table 2) the solutions approach one of the immune-present, virus-present (IV) states; (b) For $p_m = 0.57 > d_e = 0.2$, $\beta = 2 \times 10^{-11}$ and the rest of parameter values as in Table 2, the solutions approach the virus-free (VF) state; (c) For $p_m = 0.57 < d_e = 0.7$ and the rest of parameter values as in Table 2, the solutions approach the IVF steady state.

3.3. **Sensitivity to model parameters.** Since we are interested in understanding how model parameters impact viral persistence (i.e., the existence of virus-present steady states (IV)), in Figure 5 we start with the baseline parameter values from Table 2 and investigate how changes in various parameters impact $V(t)$. The initial conditions used in this Section are shown in Table 1.

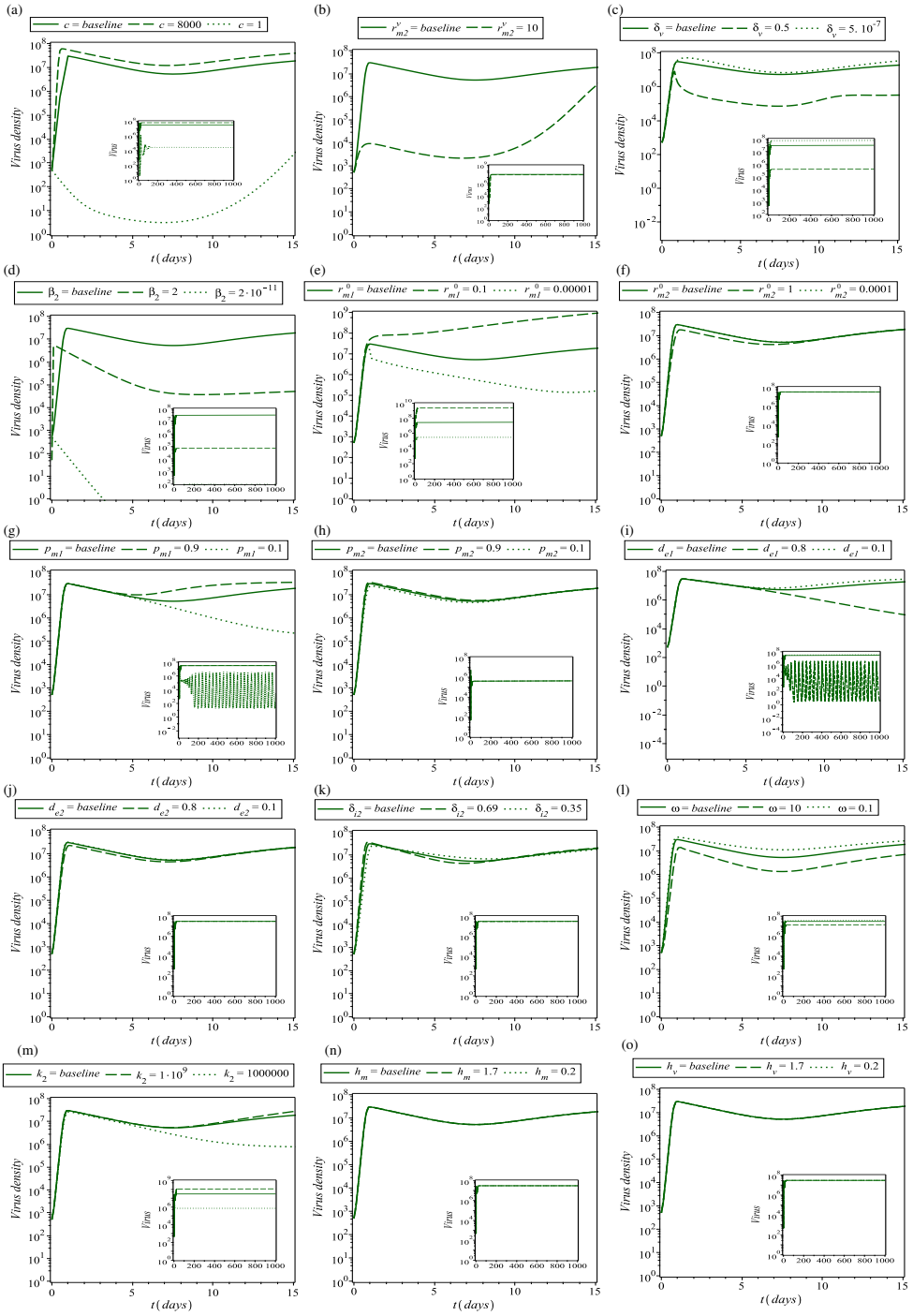

FIGURE 5. Changes in virus dynamics, $V(t)$, as we vary the following parameters: (a) burst size c; (b) virus-induced M2→M1 polarisation rate r^v_{m2}; (c) elimination rate δ_v of viruses by M1 cells; (d) macrophages infection rate β_2; (e) M1→M2 polarisation rate r^0_{m1}; (f) M2→M1 polarisation rate r^0_{m2}; (g) proliferation rate p_{m1} of M1 cells; (h) proliferation rate p_{m2} of M2 cells; (i) death rate d_{e1} of M1 cells; (j) death rate d_{e2} of M2 cells; (k) decay rate δ_{i2} of infected M2 cells; (l) virus death rate ω; (m) carrying capacity k_2 of macrophages; (n) saturation constant h_m for macrophages, (o) saturation constant h_v for virus particles. The rest of parameter values are as in Table 2. The inset figures show the long-term dynamics of $V(t)$ (i.e., for $t < 1000$ days).

In Figure 5 we see that the burst size (c), the elimination rate of the viruses by M1 cells (δ_v), the infection rate (β_2), the M1→ M2 polarisation rate (r^0_{m1}), the macrophages carrying capacity (k_2) have the greatest impact on both the short-term and long-term dynamics of virus population $V(t)$. A weaker impact is observed for the virus elimination rate (ω). Other parameters, such as r^0_{m2} or d_{e2}, impact only the transient dynamics of $V(t)$ (but not the long-term dynamics). Two other parameters, p_{m1} and d_{e1}, seem to trigger a bifurcation in the long-term dynamics of $V(t)$: from a stable steady state to a stable limit cycle (see the inset sub-figures in panels (g) and (i)). We will investigate this limit cycle in more detail in the next section.

Global sensitivity analysis. The above local sensitivity analysis examines changes in $V(t)$ based on changes in only one input parameter at a time. To investigate what happens with $V(t)$ when we change all parameter values at the same time (within the parameter ranges used for the local sensitivity), next we perform a global sensitivity analysis using the Latin Hypercube Sampling (LHS) / Partial Rank Correlation Coefficient (PRCC) approach [4, 42, 62]. In Figure 6 we show the PRCC for all model parameters. We note that only two parameters are highly and positively correlated with the viral load over the first two weeks (i.e., the PRCC value is very close to +1): β_2 (the most sensitive parameter) and c (the next sensitive parameter). A lower PRCC value is observed for δ_{i2}, and an even lower one for ω, suggesting much weaker influences of these parameters on the viral load. All other model parameters show no correlations with the output (i.e., viral load).

While both local and global sensitivity analysis identified β_2 and c as the parameters that have the greatest influence on viral load, and ω as a parameter with a weak influence on viral load, there are also some significant differences in the local/global sensitivity results. In particular, local sensitivity identified also δ_v, r^0_{m1} and k_2 as potentially important parameters, while global sensitivity identified δ_{i2} as a potentially important parameter. These differences suggest that there is a high variation in the output, especially when we are moving away from the baseline values chosen in Table 2.

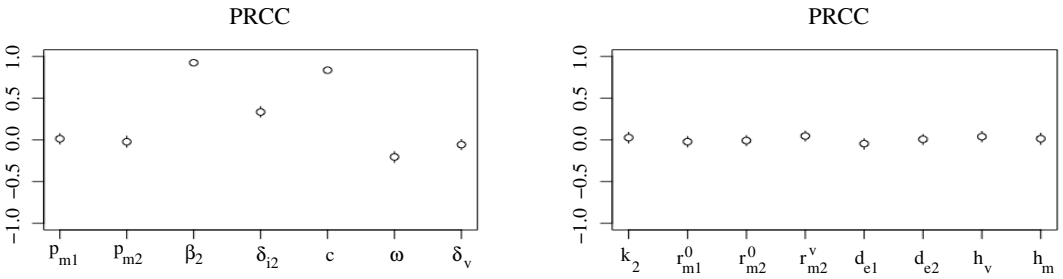

FIGURE 6. The effect of model parameters on V levels, as predicted by LHS-PRCC analysis. Each parameter is sampled randomly (1000 samples), using a uniform distribution, from the same parameter ranges used for the local sensitivity analysis (i.e., $p_{m1} \in [0.1, 0.9]$, $p_{m2} \in [0.1, 0.9]$, $\beta_2 \in [2 \times 10^{-11}, 2]$, $\delta_{i2} \in [0.35, 0.69]$, $c \in [1, 8000]$, $\omega \in [0.1, 10]$, $\delta_v \in [5 \times 10^{-7}, 0.5]$, $k_2 \in [10^6, 10^9]$, $r^0_{m1} \in [10^{-5}, 0.1]$, $r^0_{m2} \in [10^{-4}, 1]$, $r^v_{m2} \in [0, 10]$, $d_{e1} \in [0.1, 0.8]$, $d_{e2} \in [0.1, 0.8]$, $h_v, h_m \in [0.2, 1.7]$). We simulate the viral load for 14 days (similar to the time scale shown in Figure 5), with a time-step of 1 day. The PRCC index varies between -1 and $+1$; the largest PRCC (in absolute value) corresponds to the parameter to which the model outcome is most sensitive to: here β_2 and c, followed by δ_{i2} and ω. All other parameters have PRCC< 0.1.

3.4. **Oscillatory dynamics.** We now focus on the long-term oscillatory dynamics observed in Figure 5(i), which was obtained when we increased the death rate of M1 cells to $d_{e1} = 0.8$ (while keeping the

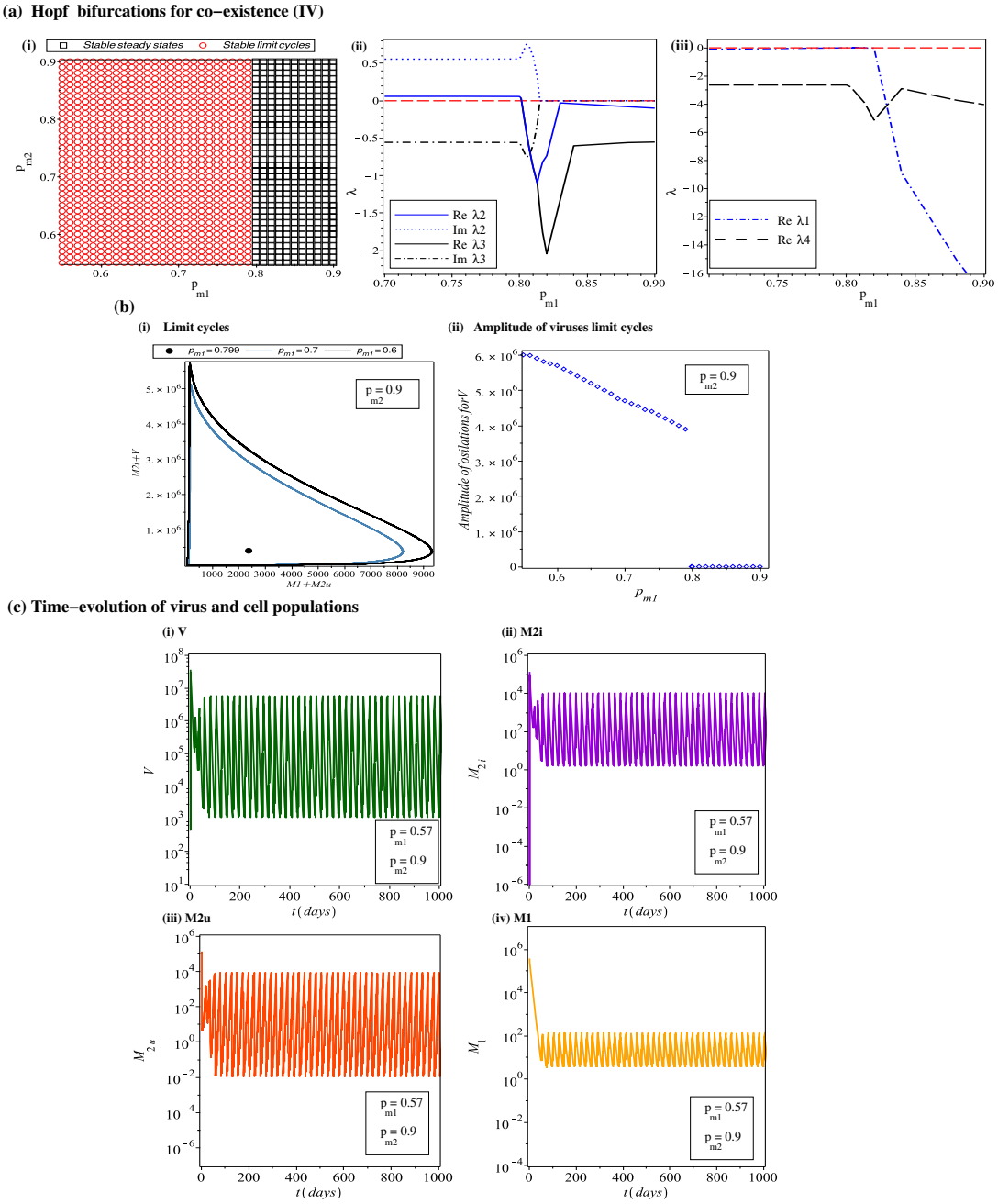

FIGURE 7. Oscillatory dynamics exhibited by model (2.1). (a) Hopf-bifurcation for the co-existence steady state (IV), when $d_{e1} = 0.8$, $d_{e2} = 0.1$ and we vary p_{m1} and p_{m2}. (i) Bifurcations between stable steady states (IV) and stable limit cycles in the (p_{m1}, p_{m2}) space; (ii),(iii) changes in the real and imaginary part of eigenvalues of the Jacobian matrix at the steady state (IV), as we vary p_{m1}. (b) (i) Limit cycles obtained for $p_{m2} = 0.9$, and different p_{m1} values; (ii) Amplitude of oscillations in $V(t)$ as we increase p_{m1}. (c) Example of oscillatory dynamics obtained for $p_{m1} = 0.57, p_{m2} = 0.9$: (i) $V(t)$, (ii) $M_{2i}(t)$, (iii) $M_{2u}(t)$, (iv) $M_1(t)$. The rest of parameter values are as described in Table 2.

death rate of M2 cells at its baseline value $d_{e2} = 0.2$). Having different macrophages death rates seems is biologically realistic. In [30] the authors noted that the murine macrophages with M1-like markers have a half-life between $18 - 20$ hrs, while the macrophages with M2-like markers have a half-life between $5 - 7$ days. This corresponds to the following death rates: $d_{e2} \in (0.099, 0.138)$ and $d_{e1} \in (0.83, 0.92)$.

In Figure 7 we assume that $d_{e1} = 0.8$ and $d_{e2} = 0.1$, and investigate the effect of varying the macrophages proliferation rates p_{m1} and p_{m2}. Note that in this case there is only one positive co-existence steady state (and not two, as for the case $d_{e1} = d_{e2} = 0.2$ and $p_{m1} = p_{m2} = 0.57$ investigated in Figure 3(a)); see also the discussion in Appendix C. Figure 7(a)(i) shows the existence of a Hopf bifurcation as we vary p_{m1}. Sub-panels (a)(ii) and (a)(iii) show the numerically-calculated real and imaginary parts of the eigenvalues λ of the Jacobian matrix, as we vary p_{m1}; here $\lambda_{1,4} \in \mathbb{R}$, $\lambda_{2,3} \in \mathbb{C}$). In Figure 7(b)(i) we graph in the $(M_1+M_{2u}, V+M_{2i})-$space the limit cycles obtained for $p_{m2} = 0.9$ and various p_{m1} values, while in Figure 7(b)(ii) we graph the changes in the amplitude of the oscillations in $V(t)$ as we vary p_{m1}. Finally, in Figure 7(c) we graph an example of the time-evolution of the oscillations in (i) $V(t)$, (ii) $M_{2i}(t)$, (iii) $M_{2u}(t)$, (iv) $M_1(t)$, for some specific p_{m1} and p_{m2} values.

3.5. **Macrophages as reservoirs for viruses.** Until now we investigated the case where VSV particles infect the M2 macrophages and replicate inside these cells (i.e., $c \gg 1$). Equation (2.1d) did not incorporate an extra term (i.e., $-\beta_2 V M_{2u}$) to account for the loss of free viruses trapped inside the M2 cells, since due to the high replication rate c such a term would not impact significantly the dynamics of system (2.1).

In the following we investigate numerically the dynamics of model (2.1) under the assumption that macrophages act as reservoirs for the virus particles [54]. In this case, we have $c = 1$ (i.e, the virus particles entering the cells do not replicate). For this reason, we need to consider a virus-trapping term to account for the removal of free virus particles from the environment, as these viruses are hiding inside the macrophages. Thus, Eq. (2.1d) now becomes:

$$\frac{dV(t)}{dt} = c\delta_{i2} M_{2i}(t) - \delta_v V(t) \frac{M_1(t)}{h_m + M_{2u}(t)} - \omega V(t) - \beta_2 V(t) M_{2u}(t).$$

Since the M2 cells are assumed to act as reservoirs, it make sense to assume also a reduction in the lysis rate δ_{i2}.

Figure 8 shows the dynamics of viruses and infected cells when: (a) $c = 2500$ and $\delta_{i2} = 0.52$ (baseline parameters; see Table 2); (b) $c = 1$ and $\delta_{i2} = 0.52$ (same lysis rate as before); (c) $c = 1$ and $\delta_{i2} = 0.052$ (low lysis rate); (d) $c = 1$ and $\delta_{i2} = 0.0052$ (very low lysis rate). We note that the assumption of M2 macrophages acting as a viral reservoir (and thus being characterised by a low lysis rate) leads to the persistence of a very low virus population, and a slightly higher infected M2 macrophage population. Further reduction in δ_{i2} (e.g., from $\delta_{i2} = 0.052$ to $\delta_{i2} = 0.0052$) does not affect the size of virus and infected macrophage populations.

4. Summary and Discussion

In this work, we have considered a mathematical modelling and computational approach to investigate the interaction between an oncolytic virus (Vesicular Stomatitis Virus – VSV) and the innate immunity generated by M1 and M2 macrophages in response to this virus. While oncolytic viruses are used in the context of tumour therapies, here we ignored the tumour and focused exclusively on the interactions between the viruses and the innate immunity (the tumour-virus-immune interactions will be investigated in a future study [2]).

First we have shown that the mathematical model for macrophages-virus interactions we developed in this study is biologically realistic, in the sense that the solutions are non-negative and bounded. Second, by focusing on the long-term dynamics of this model, we have shown that there are three types of equilibria: (i) an immune-free virus-free equilibrium, (ii) an immune-present virus free equilibrium, and (iii) multiple immune-present virus-present equilibria (see Figure 4). Since we were interested in the state where virus is present, we then investigated the changes in this co-existent state as we varied different model parameters (see Figure 5). Local and global sensitivity analysis showed that the virus

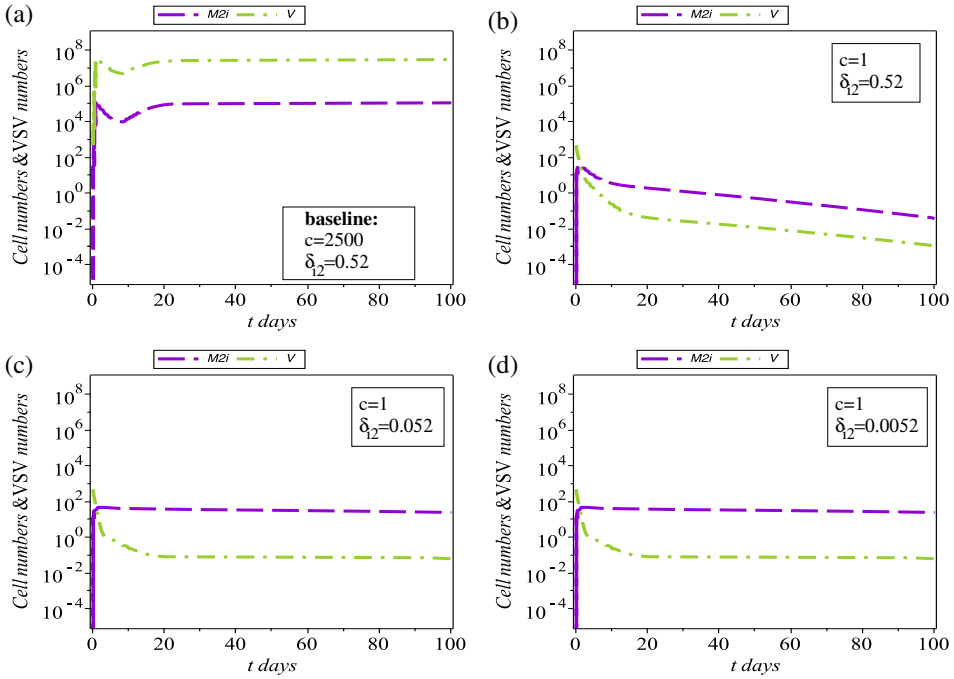

FIGURE 8. Dynamics of virus $V(t)$ and infected macrophages $M_{2i}(t)$, under the assumption that macrophages support (a) virus proliferation ($c = 2500$, $\delta_{i2} = 0.52$); (b) viral reservoir with a high virus-lysis rate ($c = 1$, $\delta_{i2} = 0.52$); (c) viral reservoir with a low lysis rate ($c = 1$, $\delta_{i2} = 0.052$); (d) (c) viral reservoir with a very low lysis rate ($c = 1$, $\delta_{i2} = 0.0052$).

population is most sensitive to the burst size c of infected cells and the infection rate β_2, and less sensitive to the virus elimination rate ω. Differences between the local and global sensitivity results for parameters δ_v, r^0_{m1}, k_2 (identified as important by local sensitivity) and δ_{i2} (identified as important by global sensitivity), are the result of model nonlinearity. Thus, some parameters are non-monotonically correlated with the viral load (i.e., $PRCC < 0.1$), while other parameters can become monotonically correlated with the viral load (i.e., $PRCC > 0.3$) only when varied inside parameter spaces where many other parameters are away from the baseline values listed in Table 2.

Finally, we investigated the role of macrophages as promotors of virus replication versus viral reservoirs (see Figure 8). We confirmed numerically the persistence of virus (and infected M2 macrophages) in the case of macrophages acting as viral reservoirs, in the context of a very low lysis rate of infected cells by viruses. The assumption of viral reservoirs was shown to lead to lower virus levels compared to the assumption of active viral replication.

Biological significance. In this study, our focus was on an oncolytic VSV, which was successful enough in reducing the size of different tumours to be allowed to reach the clinical trials stage [20]. However, one of the main problems with oncolytic viruses (including VSV) is their premature clearance by the immune response. Given that previous experimental studies have shown that VSV can infect one of the main types of immune cells infiltrating solid tumour, namely the M2 macrophages, here we focused on the poorly-understood interactions between VSV and such macrophages. As discussed above, if we assume that the M2 macrophages promote VSV replication, then parameters such as c, and β_2 lead to

an increased virus population, which is important for anti-tumour viral therapies (not considered here, but investigated in an upcoming study [2]). If, on the other hand, we assume that the M2 macrophages only act as reservoirs for viruses, there is a persistent low-level of infected macrophages and a low-level of virus particles. The level of infected M2 cells can be slightly increased if we increase the infection rate β_2 (not shown here). However, it cannot reach the level obtained under the assumption of active viral replication. Therefore, depending on the role of M2-like macrophages, one could predict lower/higher levels of virus particles in the system.

Appendix A

Proof of Proposition 3.1:
(i) The functions on the right hand side of Eqs. (2.1a)-(2.1d) are $\mathbb{C}^1$ on $\mathbb{R}^4$. Thus, it follows from the Fundamental Existence-Uniqueness Theorem for ODEs [47] that Eqns. (2.1a)-(2.1d) exhibit a unique solution that satisfies the initial conditions (2.2). □
(ii) Now we show that model (2.1a)-(2.1d) is biologically realistic, in the sense that the cell and virus populations cannot become negative. To do so, we investigate the conditions under which the non-negative orthant $\mathbb{R}^4_{\geq 0}$ is positively invariant for (2.1a)-(2.1d) (see e.g. [46]):

$$\begin{aligned}
\dot{M}_1 \mid_{(M_1=0)} &= a_1^v V + M_{2u}(r_{m2}^0 + r_{m2}^v \frac{V}{h_v + V}) \geq 0, && \text{for all } V, M_{2u} \geq 0,\\
\dot{M}_{2u} \mid_{(M_{2u}=0)} &= M_1 r_{m1}^0 \geq 0, && \text{for all } M_1 \geq 0,\\
\dot{M}_{2i} \mid_{(M_{2i}=0)} &= \beta_2 V M_{2u} \geq 0, && \text{for all } M_{2u}, V \geq 0,\\
\dot{V} \mid_{(V=0)} &= c\delta_{i2} M_{2i} \geq 0, && \text{for all } M_{2i} \geq 0.
\end{aligned}$$

Thus the non-negative orthant $\mathbb{R}^4_{\geq 0}$ is positively invariant, namely, if a trajectory starts in $\mathbb{R}^4_{\geq 0}$, it remains there for all $t \geq 0$. □

To show the boundedness of the solutions for system (2.1a)-(2.1d), we use a similar approach as in [60]. By adding Eq. (2.1a) and Eq. (2.1a), we obtain

$$\begin{aligned}
\frac{d(M_1(t) + M_{2u}(t))}{dt} &= \big(p_{m1}M_1(t) + p_{m2}M_{2u}(t)\big)\left(1 - \frac{M_1(t) + M_{2u}(t)}{k_2}\right) - \big(d_{e1}M_1(t) + d_{e2}M_{2u}(t)\big)\\
&\quad -\beta_2 V(t) M_{2u}(t)\\
&\leq \big(p_{m1}M_1(t) + p_{m2}M_{2u}(t)\big)\left(1 - \frac{M_1(t) + M_{2u}(t)}{k_2}\right),
\end{aligned}$$

which implies that $\lim_{t\to+\infty}(M_1(t) + M_{2u}(t)) \leq k_2$. For any fixed $\epsilon > 0$ let $L_1 = k_2 + \epsilon$. Then $M_1(t) + M_{2u}(t) \leq L_1$ for sufficiently large t.
Let $T(t) = M_1(t) + M_{2u}(t) + M_{2i}(t)$. Then $T(t)$ satisfies (for sufficiently large t)

$$\begin{aligned}
\frac{dT(t)}{dt} &= \big(p_{m1}M_1(t) + p_{m2}M_{2u}(t)\big)\left(1 - \frac{M_1(t) + M_{2u}(t)}{k_2}\right) - d_{e1}M_1(t) - d_{e2}M_{2u}(t) - \delta_{2i}M_{2i}(t)\\
&\leq p_{m1}\big(M_1(t) + M_{2u}(t)\big) + p_{m2}\big(M_{2u}(t) + M_1(t)\big) - \sigma\big(M_1(t) + M_{2u}(t) + M_{2i}(t)\big)\\
&\leq L_1(p_{m1} + p_{m2}) - \sigma T(t),
\end{aligned}$$

where $\sigma = \min\{d_{e1}, d_{e2}, \delta_{2i}\}$. The above inequality reduces to

$$T(t) \leq e^{-\sigma t}\left(T(0) - \frac{L_1(p_{m1} + p_{m2})}{\sigma}\right) + \frac{L_1(p_{m1} + p_{m2})}{\sigma}.$$

Hence, if $T(0) \leq L_2$ with $L_2 = \frac{L_1(p_{m1}+p_{m2})}{\sigma}$, then $0 \leq T(t) \leq L_2$ for sufficiently large t. Since $M_1(t), M_{2u}(t)$ and $M_{2i}(t)$ are all non-negative, then $M_{2i}(t) \leq L_2$, for sufficiently large t. Moreover,

because all variables are non-negative, we obtain the following inequality:

$$\frac{dV(t)}{dt} = c\delta_{i2}M_{2i}(t) - \delta_v V(t)\frac{M_1(t)}{h_m + M_{2u}(t)} - \omega V(t) \leq c\delta_{i2}L_2 - \omega V(t),$$

Hence, if $V(0) \leq L_3$ with $L_3 = \frac{c\delta_{i2}L_2}{\omega}$, then $0 \leq V(t) \leq L_3$ for sufficiently large t. □

Appendix B

Proof of Proposition 3.2: In the following we discuss the conditions for existence of the steady states $(M_1^*, M_{2u}^*, M_{2i}^*, V^*)$, when $p_{m1} = p_{m2} = p_m$ and $d_{e1} = d_{e2} = d_e$.

- It is obvious that the zero steady state $(0, 0, 0, 0)$ exists for all positive parameter values, while the immune-present virus-free state $(M_1^*, M_{2u}^*, 0, 0)$ exists only if $p_m > d_e$ (see Eq. 3.4).
- In regard to the co-existence state $(M_1^* > 0, M_{2u}^* > 0, M_{2i}^* > 0, V^* > 0)$ we note that if we add Eqns. (3.1a)+(3.1b) we obtain

$$(M_1^* + M_{2u}^*)\left((p_m - d_e) - \frac{M_1^* + M_{2u}^*}{k_2}\right) = \beta_2 V^* M_{2u}^*.$$

This equation is satisfied only if $p_m > d_e$ (since $\beta_2, V^*, M_{2u}^*, M_1^* > 0$). Moreover, the positivity of M_1^* (given by Eq. (3.3)) is ensured if $M_{2u}^* > \omega/\beta_2 c$.

Finally, since this co-existence steady state must be a root for the 4th-order polynomial given by Eq. (3.6), which connects M_{2u}^* with V^*, next we investigate the conditions that need to be satisfied by M_{2u}^* and V^* to ensure the existence of two or four such steady states.
First, we note that $A > 0$ in Eq. (3.6), and thus we have $P(M_{2u}^*) \to +\infty$ as $M_{2u}^* \to \pm\infty$. Moreover, we have $P(0) = F > 0$ for $p_m > d_e$. Therefore, to have positive roots for $P(M_{2u}^*) = 0$, this polynomial should have a negative local minimum for some $M_{2u}^* > 0$. This translates into $P'(M_{2u}^*) = 0$ for some $M_{2u}^* > 0$ (while $P(M_{2u}^*) < 0$).
Since $P'(+\infty) > 0$, if we would have $P'(0) = D + EV^* < 0$ (for $p_m > d_e$ and $c\beta_2 h_m - \omega + \delta_v > 0$), then using the Intermediate Value Theorem we could say that there is a $M_{2u}^* > 0$ such that $P'(M_{2u}^*) = 0$. Hence, condition $V^* < -D/E$ is necessary for having two positive roots M_{2u}^* of Eq. (3.6), and thus for having a non-zero co-existence steady state.

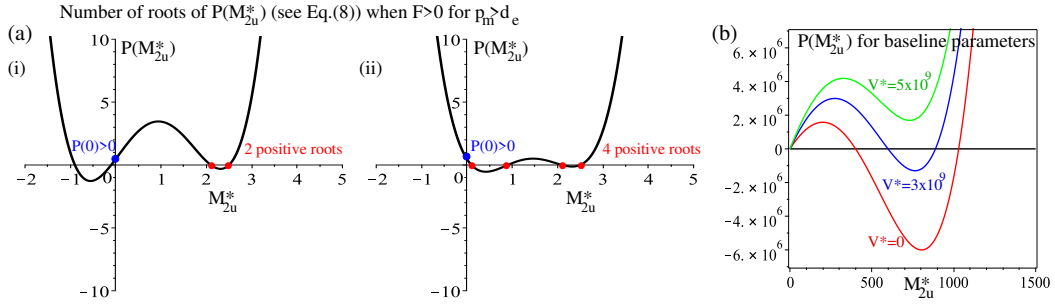

Figure 9. Description of the number of positive roots for the 4th order polynomial $P(M_{2u}^*) = 0$ (obtained when $p_{m1} = p_{m2} = p_m$ and $d_{e1} = d_{e2} = d_e$; see Eq. (3.6)). Sub-panels (a) (i),(ii) show two caricature descriptions of the number of possible roots depending on the specific parameter values in Eq. (3.6), when assuming $p_m > d_e$, and thus $P(0) = F > 0$. Sub-panel (b) shows the actual number of roots for the parameters used in this study (Table 2), as we vary the steady-state level of virus particles V^* in equation (3.6).

Now we investigate the stability of the steady states for the parameter values used in this study (when $p_{m1} = p_{m2} = p_m$, $d_{e1} = d_{e2} = d_e$). The Jacobian matrix associated with system (2.1a)-(2.1d) at a

general equilibrium point is:

$$J(M_1^*, M_{2u}^*, M_{2i}^*, V^*) = \begin{bmatrix} a_{11} & a_{12} & a_{13} & a_{14} \\ a_{21} & a_{22} & a_{23} & a_{24} \\ a_{31} & a_{32} & a_{33} & a_{34} \\ a_{41} & a_{42} & a_{43} & a_{44} \end{bmatrix}, \tag{4.1}$$

with

$a_{11} = p_{m1}\left(1 - \frac{M_1^*+M_{2u}^*}{k_2}\right) - \frac{p_{m1}M_1^*}{k_2} - r_{m1}^0 - d_{e1}$, $a_{12} = r_{m2}^0 + \frac{r_{m2}^v V^*}{h_v+V^*} - \frac{p_{m1}M_1^*}{k_2}$, $a_{13} = 0$,

$a_{14} = M_{2u}^*\left(\frac{r_{m2}^v}{h_v+V^*} - \frac{r_{m2}^v V^*}{(h_v+V^*)^2}\right)$, $a_{21} = r_{m1}^0 - \frac{p_{m2}M_{2u}^*}{k_2}$,

$a_{22} = p_{m2}\left(1 - \frac{M_1^*+M_{2u}^*}{k_2}\right) - \frac{p_{m2}M_{2u}^*}{k_2} - \frac{r_{m2}^v V^*}{h_v+V^*} - \beta_2 V^* - r_{m2}^0 - d_{e2}$, $a_{23} = 0$,

$a_{24} = M_{2u}^*\left(\frac{r_{m2}^v V^*}{(h_v+V^*)^2} - \frac{r_{m2}^v}{h_v+V^*}\right) - \beta_2 M_{2u}^*$, $a_{31} = 0$, $a_{32} = \beta_2 V^*$, $a_{33} = -\delta_{i2}$, $a_{34} = \beta_2 M_{2u}^*$,

$a_{41} = -\frac{\delta_v V^*}{h_m+M_{2u}^*}$, $a_{42} = \frac{\delta_v V^* M_1^*}{(h_m+M_{2u}^*)^2}$, $a_{43} = c\delta_{i2}$, $a_{44} = -\omega - \frac{\delta_v M_1^*}{h_m+M_{2u}^*}$.

Next we investigate the eigenvalues of this Jacobian at the specific steady states exhibited by model (2.1):

(i) *Immune-Free Virus-Free Steady State* (IVF): The eigenvalues of the Jacobian matrix (4.1) calculated at $(0,0,0,0)$ are: $\lambda_1 = -\omega < 0$, $\lambda_2 = -\delta_{i2} < 0$, and $\lambda_{3,4}$ satisfying the following equation

$$\lambda^2 - \lambda(a_{11} + a_{22}) + a_{11}a_{22} - a_{12}a_{21} = 0$$

with

$$a_{11} = p_{m1} - r_{m1}^0 - d_{e1}, \quad a_{22} = p_{m2} - r_{m2}^0 - d_{e2}, \quad a_{12} = r_{m2}^0, \quad a_{21} = r_{m1}^0.$$

This zero steady state is stable if $a_{11}+a_{22} < 0$ and $a_{11}a_{22} - a_{12}a_{21} > 0$, which for $p_{m1} = p_{m2} := p_m$ and $d_{e1} = d_{e2} := d_e$ (as assumed throughout most of the manuscript) reduce to

$$p_m - d_e < \frac{1}{2}(r_{m1}^0 + r_{m2}^0), \quad \text{and} \quad \left[p_m - d_e - (r_{m1}^0 + r_{m2}^0)\right][p_m - d_e] > 0. \tag{4.2}$$

These two inequalities hold true when $d_e > p_m$.

When $p_m = d_e$ the eigenvalues of the Jacobian matrix calculated at this trivial steady state are: $\lambda_1 = -\omega$, $\lambda_2 = -\delta_{i2}$, $\lambda_3 = -(r_{m1}^0 + r_{m2}^0)$, $\lambda_4 = 0$. Since the trivial state is now a non-hyperbolic equilibrium, we investigate its stability with the help of a Lyapunov function. To this end consider the following function:

$$L(M_1, M_{2u}, M_{2i}, V) = M_1 + M_{2u} + M_{2i} + \frac{1}{c}V.$$

Clearly, $L(0,0,0,0) = 0$ and $L(M_1, M_{2u}, M_{2i}, V) > 0$ for $M_1, M_{2u}, M_{2i}, V > 0$ (see Proposition 3.1). Moreover,

$$\begin{aligned} L'(M_1, M_{2u}, M_{2i}, V) &= M_1' + M_{2u}' + M_{2i}' + \frac{1}{c}V' \\ &= -\frac{p_m}{k_2}(M_1 + M_{2u})^2 - \frac{\delta_v}{c}V\frac{M_1}{h_m + M_{2u}} - \frac{\omega}{c}V \le 0, \end{aligned}$$

since $M_1, M_{2u}, M_{2i}, V \ge 0$. In fact $L' < 0$ if $M_1, M_{2u}, M_{2i}, V > 0$. Therefore L satisfies the conditions of a Lyapunov function, and thus $(0,0,0,0)$ is asymptotically stable also for $p_m = d_e$.

(ii) *Immune-Present Virus-Free Steady State* (VF): $(M_1^*, M_{2u}^*, 0, 0)$, where

$$M_1^* = \frac{(p_m - d_e)k_2 r_{m2}^0}{(r_{m1}^0 + r_{m2}^0)p_m}, \quad M_{2u}^* = \frac{(p_m - d_e)k_2 r_{m1}^0}{(r_{m1}^0 + r_{m2}^0)p_m}, \quad \text{exists for } p_m > d_e. \tag{4.3}$$

The four eigenvalues of the Jacobian matrix (4.1) associated with system (2.1a)-(2.1d) and calculated at this state are satisfying two quadratic equations:

– The first equation is

$$\lambda^2 - \lambda(c_{11} + c_{22}) + c_{11}c_{22} - c_{12}c_{21} = 0,$$

with

$$c_{11} = \frac{(d_e - pm - r^0_{m1})r^0_{m2} - (r^0_{m1})^2}{(r^0_{m1} + r^0_{m2})}, \quad c_{12} = \frac{(d_e - p_m)r^0_{m2}}{(r^0_{m1} + r^0_{m2})} + r^0_{m2},$$
$$c_{21} = \frac{(d_e - p_m)r^0_{m1}}{(r^0_{m1} + r^0_{m2})} + r^0_{m1}, \quad c_{22} = \frac{(d_e - pm - r^0_{m2})r^0_{m1} - (r^0_{m2})^2}{(r^0_{m1} + r^0_{m2})}.$$

The roots $\lambda_{1,2}$ are negative provided that $c_{11} + c_{22} < 0$ and $c_{11}c_{22} - c_{12}c_{21} > 0$. These two inequalities can be re-written as

$$d_e - p_m - r^0_{m1} - r^0_{m2} < 0, \quad \text{and} \quad (p_m - d_e)(r^0_{m1} + r^0_{m2}) > 0,$$

which hold true if $p_m > d_e$ (when this virus-free steady state exists).

– The second quadratic equation (which gives us $\lambda_{3,4}$) is

$$\lambda^2 - b_1\lambda + b_2 = 0,$$

with

$$b_1 = -\omega - \delta_{i2} - \frac{\delta_v M^*_1}{h_m + M^*_{2u}}, \; b_2 = \delta_{i2}\left(\omega + \frac{\delta_v M^*_1}{h_m + M^*_{2u}} - c\beta_2 M^*_{2u}\right).$$

Since b_1 is always negative, the stability of this steady state depends on the value of b_2: if $b_2 > 0$ then this steady state is stable. One can re-write this condition as

$$b_2 = -\delta_{i2}\left(R^0_e - 1\right), \quad \text{with} \quad R^0_e = \frac{c\beta_2 M^*_{2u}}{\delta_v \frac{M^*_1}{h_m + M^*_{2u}} + \omega}.$$

For the parameters used in this study $R^0_e > 1$, which implies that $b_2 < 0$ and thus this equilibrium is unstable.

(iii) *Immune-Present Virus-Present Steady States* (IV): given that the Jacobian matrix calculated at the states $(M^{*,v}_1, M^{*,v}_{2u}, M^{*,v}_{2i}, V^{*,v})$ is very complex, and we could not find explicit solutions for these co-existence states (see Eq. (3.6) and Figure 2), the stability of these states is even more difficult to be investigated analytically. Thus we calculate numerically (for the baseline parameters listed in Table 2) the eigenvalues of the Jacobian matrix corresponding to the two steady states shown in Figure 2. Figure 10(a) shows one more time these two steady states as we vary: (a) V^* (while keeping all parameter values, including p_m, fixed at their baseline levels from Table 2); (b) p_m (while fixing $V^* = 2 \times 10^9$ and all other parameters at their baseline levels). Sub-panel (b)(ii) shows the eigenvalues of the Jacobian matrix at the state $M^{*,1}_{2u}$ (which is always stable for $p_m > 0.4218$, as all $\lambda_i < 0$, $i = 1, 2, 3, 4$). Sub-panel (b)(iii) shows the eigenvalues of the Jacobian matrix at the state $M^{*,2}_{2u}$ (which turns out to be stable for $p_m \leq 0.433$ and unstable for $p_m > 0.433$ – when $\lambda_4 > 0$).

Appendix C

Conditions for the co-existence steady state when $\mathbf{p_{m1} \neq p_{m2}, d_{e1} \neq d_{e2}}$. In Section 3.4 we investigated numerically the case when $p_{m1} \neq p_{m2}$ and $d_{e1} \neq d_{e2}$. In the following we study the conditions for the existence and the number of coexistence steady states $(M^*_1, M^*_{2u}, M^*_{2i}, V^*)$ for this particular case.

When $p_{m1} \neq p_{m2}$ and $d_{e1} \neq d_{e2}$, the co-existence steady state is a root for the 4th-order polynomial given by the following equation:

$$Q(M^*_{2u}) := A(M^*_{2u})^4 + B(M^*_{2u})^3 + C(M^*_{2u})^2 + (D + EV^*)(M^*_{2u}) + F = 0, \tag{4.4}$$

where

$$A = p_{m1}c^2\beta_2^2, \quad B = c\beta_2\left(2(\beta_2 c h_m - \omega)p_{m1} + \delta_v(p_{m1} + p_{m2})\right),$$

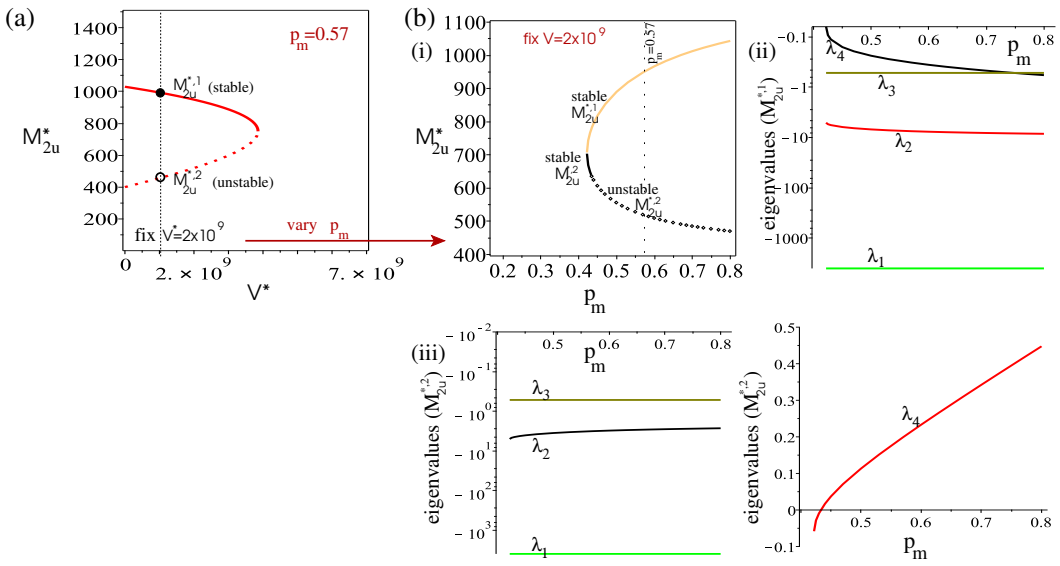

FIGURE 10. (a) Stability of Immune-Present Virus-Present steady states (IV) as we vary V^*; here we fix $p_m = 0.57$, $d_e = 0.2$. (b) Stability of Immune-Present Virus-Present steady states (IV) as we fix $V^* = 2 \times 10^9$ and we vary p_m. The dotted vertical line identifies the value $p_m = 0.57$ used in sub-panel (a). Sub-panel (b)(i) shows the existence of stable/unstable states $M_{2u}^{*,1}$ and $M_{2u}^{*,2}$ as we vary p_m; note that for $p_m \in (0.4218, 0.433)$ both steady states are stable, while for $p_m > 0.433$ the first state ($M_{2u}^{*,1}$) is stable while the second state ($M_{2u}^{*,2}$) is unstable. Sub-panels (ii) and (iii) show the eigenvalues of the Jacobian matrix (4.1) at each of these two (IV) states, which determine the stability of the two steady-state branches shown in sub-panel (i).

$$C = p_{m2}\delta_v^2 + [c\,((h_m - k_2)p_{m1} + h_m p_{m2} + d_{e1}k_2)\,\beta_2 - \omega(p_{m1} + p_{m2})]\,\delta_v + p_{m1}(\beta_2^2 c^2 h_m^2 - 4\beta_2 c h_m \omega + \omega^2),$$
$$D = (d_{e2} - p_{m2}) - ((p_{m1} - d_{e1})(\beta_2 c h_m - \omega)k_2 + \omega h_m(p_{m1} + p_{m2}))\,\delta_v + 2\omega h_m p_{m1}(\beta_2 c h_m - \omega),$$
$$E = \beta_2 k_2 \delta_v^2, \qquad F = h_m\omega\,(k_2(p_{m1} - d_{e1})\delta_v + \omega h_m p_{m1})\,.$$

As for Eq. (3.6) we have $A > 0$ and therefore $Q(M_{2u}^*) \to \infty$ as $M_{2u}^* \to \infty$. If we vary p_{m1} above/below d_{e1} value, as in Figure 7, we note that F could be positive or negative:

- for $d_{e1} = 0.8$, $p_{m1} > 0.8$: we have $F > 0$, which leads to either 2 or 4 positive roots for $Q(M_{2u}^*) = 0$; same as in Figure 9 (not shown here).
- for $d_{e1} = 0.8$, $p_{m1} < 0.8$: we have $F < 0$, which leads to either 1 or 3 positive roots for $Q(M_{2u}^*) = 0$; same as in Figure 11.

However, not all these positive roots lead to biologically realistic steady states, since we also require that $M_1^* > 0$, which happens for $M_{2u}^* > \omega/(c\beta_2) = 400$ (for the parameter values used in this study: $\omega = 2$, $c = 2500$, $\beta_2 = 2 \times 10^{-6}$). Therefore, the increase in p_{m1} above d_{e1} leads to a bifurcation from 1 co-existence steady state (for $p_{m1} < d_{e1}$) to 2 co-existence steady states (for $p_{m1} > d_{e1}$). We remark that the co-existence state obtained for $p_{m1} < d_{e1}$ is characterised by a lower level of virus particles V^*, compared to the co-existence states obtained for $p_{m1} > d_{e1}$.

REFERENCES

[1] P. Allavena, A. Sica, C. Garlanda and A. Mantovani, The yin-yang of tumor-associated macrophages in neoplastic progression and immune surveillance, *Immunological Reviews* **222** (2008) 155–161.

[2] N. Almuallem and R. Eftimie, Oncolytic viral therapies and the delicate balance between virus-macrophage-tumour interactions: a mathematical approach, 2020, in preparation.

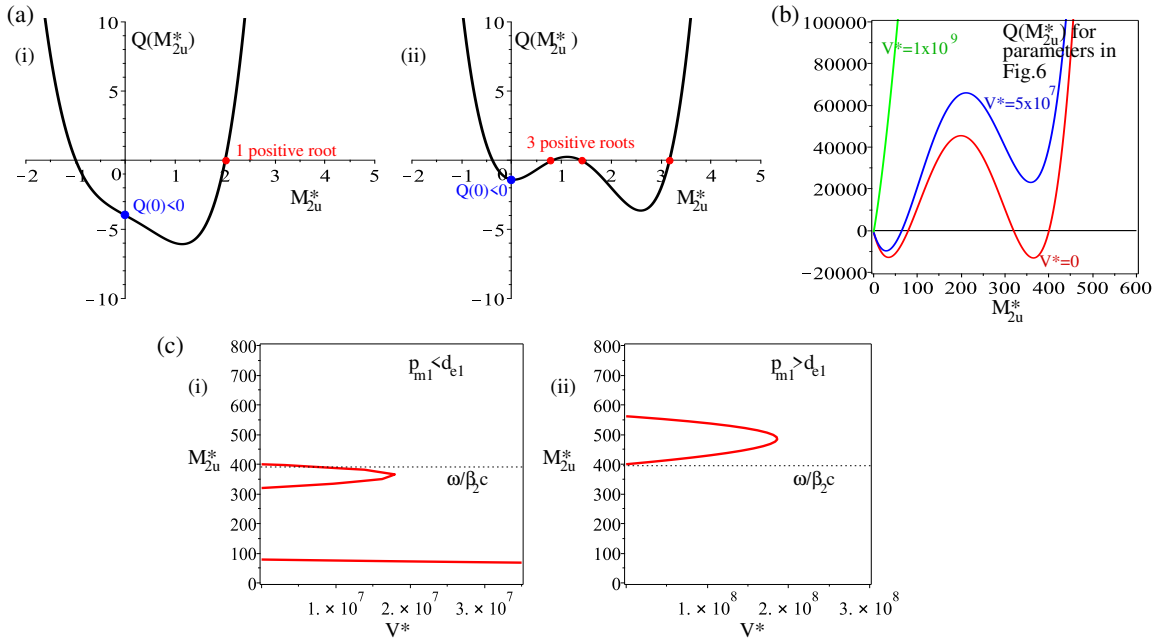

FIGURE 11. Description of the number of positive roots for the 4th order polynomial $Q(M_{2u}^*) = 0$ (obtained when $p_{m1} \neq p_{m2}$ and $d_{e1} \neq d_{e2}$; see Eq. (4.4)). Sub-panels (a) (i),(ii) show two caricature descriptions of the number of possible roots depending on the specific parameter values in Eq. (4.4), when assuming $p_{m1} = 0.78 < d_{e1} = 0.8$, and thus $Q(0) = F < 0$. Sub-panel (b) shows the actual number of roots for the parameters used in Section 3.4, as we vary the steady-state level of virus particles V^* in equation (3.6). Sub-panels (c) show the steady states M_{2u}^* vs. V^* for (i) $p_{m1} = 0.78 < d_{e1} = 0.8$, and (ii) $p_{m1} = 0.88 > d_{e2} = 0.8$, together with the dotted threshold line $M_{2u}^* = \omega/(\beta_2 c)$ which determines the existence of $M_1^* > 0$ (see also Eq. (3.3)).

[3] S. Bishnoi, R. Tiwari, S. Gupta, S. N. Byrareddy and D. Nayak, Oncotargeting by vesicular stomatitis virus (vsv): advances in cancer therapy, *Viruses* **10** (2018) 90.
[4] S. Blower and H. Dowlatabadi, Sensitivity and uncertainty analysis of complex models of disease transmission: an HIV model, as an example, *International Statistical Review* **62** (1994) 229–243.
[5] G. Bocharov and A. Romanyukha, Mathematical model of antiviral immune response III. Influenza A virus infection, *Journal of Theoretical Biology* **167** (1994) 323–360.
[6] G. Chan, E. Bivins-Smith, M. Smith, P. Smith and A. Yurochko, Transcriptome analysis reveals human cytomegalovirus reprograms monocyte differentiation toward an M1 macrophage, *Journal of Immunology* **181** (2008) 698–711.
[7] V. Chitu, Y.-G. Yeung, W. Yu, S. Nandi and E. R. Stanley, Measurement of macrophage growth and differentiation, *Current Protocols in Immunology* **92** (2011) 14–20.
[8] M. Cobleigh, C. Bradfield, Y. Liu, A. Mehta and M. Robek, The immune response to a Vesicular Stomatitis Virus vaccine vector is independent of particulate antigen secretion and protein turnover rate, *Journal of Virology* **86** (2012) 4253–4261.
[9] N. den Breems and R. Eftimie, The re-polarisation of M2 and M1 macrophages and its role on cancer outcomes, *Journal of Theoretical Biology* **390** (2016) 23–39.
[10] N. Denton, C.-Y. Chen, T. Scott and T. Cripe, Tumor-associated macrophages in oncolytic virotherapy: friend or foe?, *Biomedicines* **4** (2016) 13.
[11] N. DePolo and J. Holland, The intracellular half-lives of nonreplicating nucleocapsids of DI particles of wild type and mutant strains of vesicular stomatitis virus, *Virology* **151** (1986) 371–378.
[12] I. Dutry, J. Li, P. Li, R. Bruzzone, J. Peiris and M. Jaume, The effects of macrophage polarity on influenza virus replication and innate immune responses, *Journal of Clinical & Cellular Immunology* **6** (2015) 297.

[13] R. Eftimie and G. Eftimie, Tumour-associated macrophages and oncolytic virotherapies: a mathematical investigation into a complex dynamics, *Letters in Biomathematics* **5** (2018) S6–S35.
[14] R. Eftimie and G. Eftimie, Investigating macrophages plasticity following tumour–immune interactions during oncolytic therapies, *Acta Biotheoretica* (2019) 1–39.
[15] R. Eftimie and H. Hamam, Modelling and investigation of the CD4+ T cells–macrophages paradox in melanoma immunotherapies, *Journal of Theoretical Biology* **420** (2017) 82–104.
[16] R. Eftimie, C. K. Macnamara, J. Dushoff, J. L. Bramson and D. J. Earn, Bifurcations and chaotic dynamics in a tumour-immune-virus system, *Mathematical Modelling of Natural Phenomena* **11** (2016) 65–85.
[17] A. Elaiw, Global stability analysis of humoral immunity virus dynamics model including latently infected cells, *Journal of Biological Dynamics* **9** (2015) 215–228.
[18] A. Elaiw, N. Almuallem and A. Hobiny, Effect of RTI drug efficacy on the hiv dynamics with cocirculating target cells., *Journal of Computational Analysis & Applications* **23** (2017) 209–228.
[19] I. Elzenga-Claasen, M. D. Diesselhoff-den, H. Toivonen, T. Rytömaa et al., Cell kinetic analysis of a murine macrophage cell line., *European Journal of Cell Biology* **44** (1987) 93–96.
[20] S. Felt and V. Grdzelishvili, Recent advances in vesicular stomatitis virus-based oncolytic virotherapy: a 5-year update, *Journal of General Virology* **98** (2017) 2895–2911.
[21] A. Friedman and N. Siewe, Chronic hepatitis B virus and liver fibrosis: a mathematical model, *PLoS ONE* **13** (2018) e0195037.
[22] R. Fuller, Response of M2 macrophages in a simulated tumor microenvironment to infection with vesicular stomatitis virus, Master's thesis, Appalachian State University, 2018.
[23] Y. Gao, P. Whitaker-Dowling, S. Watkins, J. Griffin and I. Bergman, Rapid adaptation of a recombinant vesicular stomatitis virus to a targeted cell line, *Journal of Virology* **80** (2006) 8603–8612.
[24] C. Guiducci, A. P. Vicari, S. Sangaletti, G. Trinchieri and M. P. Colombo, Redirecting in vivo elicited tumor infiltrating macrophages and dendritic cells towards tumor rejection, *Cancer Research* **65** (2005) 3437–3446.
[25] M. Hadjiandreou, R. Conejeros and V. Vassiliadis, Towards a long-term model construction for the dynamic simulation of HIV infection, *Mathematical Biosciences and Engineering* **4** (2007) 489–504.
[26] E. Hastie and V. Grdzelishvili, Vesicular stomatitis virus as a flexible platform for oncolytic virotherapy against cancer, *Journal of General Virology* **93** (2012) 2529–2545.
[27] G. Herbein and A. Varin, The macrophage in HIV-1 infection: from activation to deactivation?, *Retrovirology* **7** (2010) 33.
[28] E. Hernandez-Vargas and R. Middleton, Modelling the three stages in HIV infection, *Journal of Theoretical Biology* **320** (2013) 33–40.
[29] M. Hussein, Tumour-associated macrophages and melanoma tumourigenesis: integrating the complexity, *International Journal of Experimental Pathology* **87** (2006) 163–176.
[30] P. Italiani and D. Boraschi, From monocytes to m1/m2 macrophages: phenotypical vs. functional differentiation, *Frontiers in Immunology* **5** (2014) 514.
[31] A. Klepper and A. Branch, Macrophages and the viral dissemination super highway, *EC Microbiol.* **2** (2015) 328–336.
[32] P. Lang, M. Recher, N. Honke, S. Scheu, S. Borkens, N. Gailus, C. Krings, A. Meryk, A. Kulawik, L. Cervantes-Barragan, N. V. Rooijen, U. Kalinke, B. Ludewig, H. Hengartner, N. Harris, D. Häussinger, P. Ohashi, R. Zinkernagel and K. Lang, Tissue macrophages suppress viral replication and prevent severe immunopathology in an Interferon-I-dependent manner in mice, *Hepatology* **52** (2010) 25–32.
[33] C. Larocca and J. Schlom, Viral vector-based therapeutic cancer vaccines, *Cancer J.* **17** (2011) 359–371.
[34] J. Lee, F. Adler and P. Kim, A mathematical model for the macrophage response to respiratory viral infection in normal and asthmatic conditions, *Bulletin of Mathematical Biology* **79** (2017) 1979–1998.
[35] F. Leonard, L. Curtis, M. Ware, T. Nosrat, X. Liu, K. Yokoi, H. Frieboes and B. Godin, Macrophage polarization contributes to the anti-tumoral efficacy of mesoporous nanovectors loaded with albumin-bound paclitaxelolarization contributes to the anti-tumoral efficacy of mesoporous nanovectors loaded with albumin-bound paclitaxel, *Frontiers in Immunology* **8** (2017) 693.
[36] D. Longo and L. Baden, Exploiting viruses to treat diseases, *The New England J.ournal of Medicine* **379** (2018) 194–196.
[37] Y. Louzoun, C. Xue, G. Lesinski and A. Friedman, A mathematical model for pancreatic cancer growth and treatments, *Journal of Theoretical Biology* **351** (2014) 74–82.
[38] E. G. Lucero, The cytotoxic effects of vesicular stomatitis virus on the THP-1 macrophages, 2018.
[39] C. Macnamara and R. Eftimie, Memory versus effector immune responses in oncolytic virotherapies, *Journal of Theoretical Biology* **377** (2015) 1–9.
[40] G. Magombedze, S. Eda and V. V. Ganusov, Competition for antigen between Th1 and Th2 responses determines the timing of the immune response switch during mycobaterium avium subspecies paratuberulosis infection in ruminants, *PLoS Computational Biology* **10** (2014) e1003414.
[41] G. Marchuk, A. Romanyukha and G. Bocharov, Mathematical model of antiviral immune response II. Parameters identification for acute Viral Hepatitis B, *Journal of Theoretical Biology* **151** (1991) 41–70.

[42] S. Marino, I. Hogue, C. Ray and D. Kirschner, A methodology for performing global uncertainty and sensitivity analysis in systems biology, *Journal of Theoretical Biology* **254** (2008) 178–196.
[43] M. Nicol and B. Dutia, The role of macrophages in influenza A virus infection, *Future Virology* **9**.
[44] E. Nikitina, I. Larionova, E. Choinzonov and J. Kzhyshkowska, Monocytes and macrophages as viral targets and reservoirs, *International Journal of Molecular Sciences* **19** (2018) 2821.
[45] C. Passaro, F. Borriello, V. Vastolo, S. D. Somma, E. Scamardella, V. Gigantino, R. Franco, G. Marone and G. Portella, The oncolytic virus d/922-947 reduces IL-8/CXCL8 and MCP-1/CCL2 expression and impairs angiogenesis and macrophage infiltration in anaplastic thyroid carcinoma, *Oncotarget* **7** (2016) 1500–1515.
[46] A. S. Perelson, D. E. Kirschner and R. De Boer, Dynamics of HIV infection of CD4+ T cells, *Mathematical Biosciences* **114** (1993) 81–125.
[47] L. Perko, *Differential equations and dynamical systems*, volume 7 (Springer Science & Business Media, 2013).
[48] M. A. Polzin, Therapuetic targeting of macrophage populations by oncolytic vesicular stomatitis virus, Master's thesis, Appalachian State University, 2017.
[49] R. Prestwich, F. Errington, K. Harrington, H. Pandha, P. Selby and A. Melcher, Oncolytic viruses: do they have a role in anti-cancer therapy?, *Clin. Med. Oncol.* **2** (2008) 83–96.
[50] B. Rager-Zisman, M. Kunkel, Y. Tanaka and B. R. Bloom, Role of macrophage oxidative metabolism in resistance to vesicular stomatitis virus infection., *Infection and Immunity* **36** (1982) 1229–1237.
[51] M. Robert-Guroff, Replicating and non-replicating viral vectors for vaccine development, *Curr. Opin. Biotechnol.* **18** (2007) 546–556.
[52] Y. Sang, L. C. Miller and F. Blecha, Macrophage polarization in virus-host interactions, *Journal of Clinical & Cellular Immunology* **6**.
[53] L.-M. Schreiber, C. Urbiola, K. Das, B. Spiesschaert, J. Kimpel, F. Heinemann, B. Stierstorfer, P. Müller, M. Petersson, P. Erlmann et al., The lytic activity of vsv-gp treatment dominates the therapeutic effects in a syngeneic model of lung cancer, *British Journal of Cancer* (2019) 1–12.
[54] I. Simon, N. van Rooijen and J. Rose, Vesicular stomatitis virus genomic RNA persists *in vivo* in the absence of viral replication, *Journal of Virology* **84** (2010) 3280–3286.
[55] B. Simovic, S. Walsh and Y. Wan, Machanistic insights into the oncolytic activity of vesicular stomatitis virus in cancer immunotherapy, *Oncolytic Virotherapy* **4** (2015) 157–167.
[56] S. Sousa, R. Brion, M. Lintunen, P. Kronqvist, J. Sandholm, J. Mönkkönen, D. Heymann and J. Määttä, Human breast cancer cells educate macrophages toward the M2 activation status, *Breast Cancer Research* **17**.
[57] B. Vincenzi, M. Fioramonti, M. Iuliani, F. Pantano, G. Ribelli, D. Santini and G. Tonini, M1-polarized macrophages as predictor of poor response to trabectedin treatment in myxoid liposarcoma., *Journal of Clinical Oncology* **34** (2016) e22537–e22537.
[58] S. Waggoner, S. Reighard, I. Gyurova, S. Cranert, S. Mahl, E. Karmele, J. McNally, M. Moran, T. Brooks, F. Yaqoob and C. Rydyznski, Roles of natural killer cells in antiviral immunity, *Curr. Opin. Virol.* **16** (2016) 15–23.
[59] Y. Wang, T. Yang, Y. Ma, G. V. Halade, J. Zhang, M. L. Lindsey and Y.-F. Jin, Mathematical modeling and stability analysis of macrophage activation in left ventricular remodeling post-myocardial infarction, *BMC Genomics* **13** (2012) S21.
[60] Z. Wang, Z. Guo and H. Smith, A mathematical model of oncolytic virotherapy with time delay, *Mathematical Biosciences and Engineering* **16** (2019) 1863–1860.
[61] D. Wodarz, A. Lloyd, V. Jansen and M. Nowak, Dynamics of macrophage and T cell infection by hiv, *Journal of Theoretical Biology* **196** (1999) 101–113.
[62] J. Wu, R. Dhingra, M. Gambhir and J. Remais, Sensitivity analysis of infectious disease models: methods, advances and their application, *J.R. Soc. Interface* **10** (2013) 20121018.
[63] S. Yona, K.-W. Kim, Y. Wolf, A. Mildner, D. Varol, M. Breker, D. Strauss-Ayali, S. Viukov, M. Guilliams, A. Misharin et al., Fate mapping reveals origins and dynamics of monocytes and tissue macrophages under homeostasis, *Immunity* **38** (2013) 79–91.
[64] Y.-L. Zhao, P.-X. Tian, F. Han, J. Zheng, X.-X. Xia, W.-J. Xue, X.-M. Ding and C.-G. Ding, Comparison of the characteristics of macrophages derived from murine spleen, peritoneal cavity, and bone marrow, *J. Zhejiang Univ. Sci. B* **18** (2017) 1055–1063.
[65] Y. Zhu, A. Yongky and J. Yin, Growth of an RNA virus in single cells reveals a broad fitness distribution, *Virology* **385** (2009) 39–46.
[66] J. C. Zhuang and G. N. Wogan, Growth and viability of macrophages continuously stimulated to produce nitric oxide, *Proceedings of the National Academy of Sciences* **94** (1997) 11875–11880.

Division of Mathematics, School of Science and Engineering, University of Dundee, Dundee, DD1 4HN, UK

E-mail address: n.a.s.z.almuallem@dundee.ac.uk

Corresponding author. Division of Mathematics, School of Science and Engineering, University of Dundee, Dundee, DD1 4HN, UK

E-mail address: r.a.eftimie@dundee.ac.uk